CHAPTER 4 MODELLING AND SIMULATION

This chapter shows the conceptual framework of modelling and simulation of supercritical fluid extraction systems studied in this work (Figure 4.1). This research extended the work of Ajchariyapagorn (2007), which studied supercritical fluid extraction of biomolecules with cosolvents. This chapter was structured as follows. First, physical properties estimation was addressed in section 4.1. Then, solubility modelling results in four case studies were presented and discussed in section 4.2. In section 4.3, the supercritical fluids extraction modelling results were provided in 3 subsections: (a) model validation, (b) parametric study (sensitivity analysis) and (c) extractor configuration. The supercritical fluid extraction model was developed and validated against experimental data with various operating conditions. Sensitivity analysis was performed to study effects of different transport parameters on extraction yield. Finally, extractor configuration was also investigated in order to obtain the maximum yield.

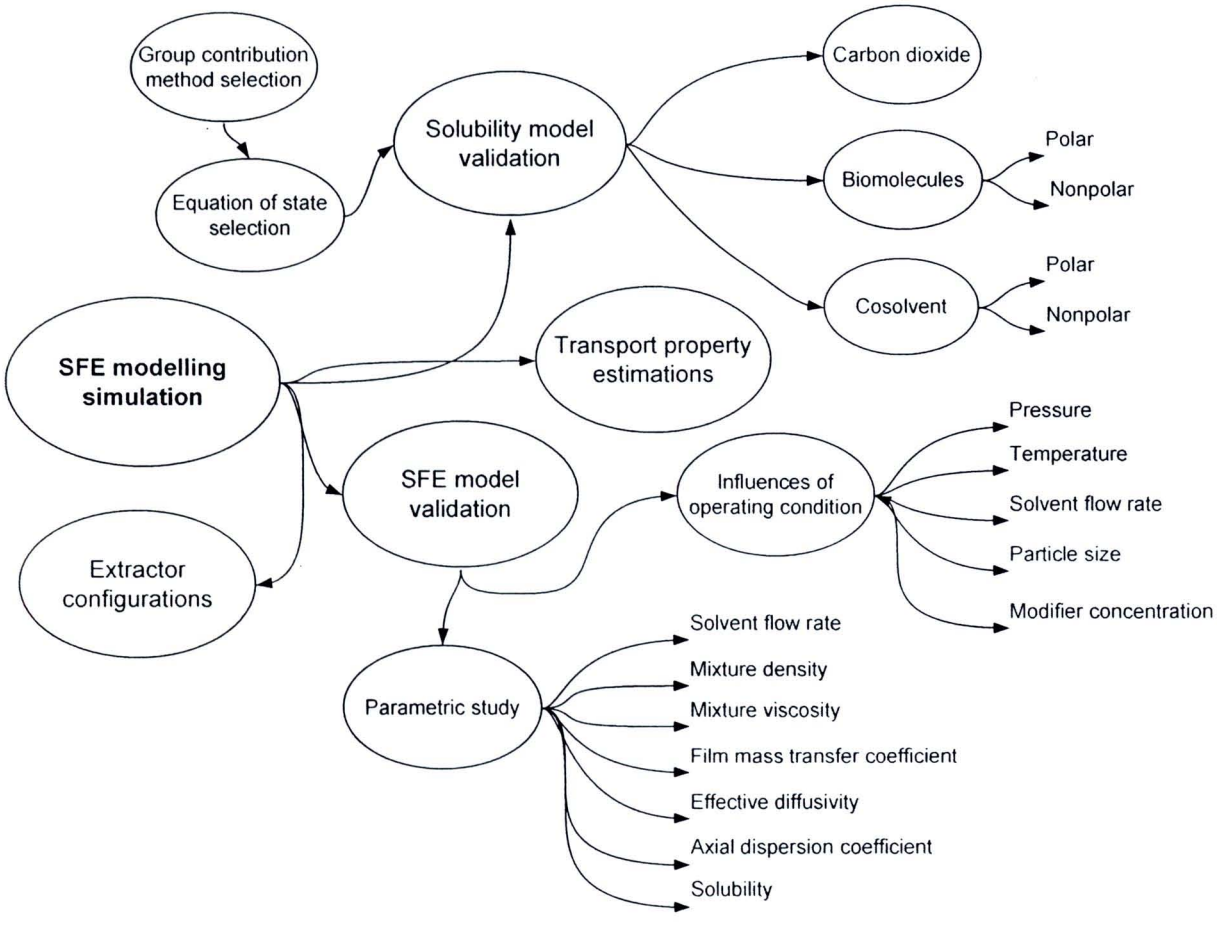

Figure 4.1 Conceptual of supercritical fluid extraction modelling and simulation.

4.1 Physical Property Estimation

The aim of this section was to provide accurate information or prediction for physical-chemical properties of all substances used in this work. Molecular structures of compounds should be known beforehand. Group contribution methods (GCMs) are available for estimating physical properties of compounds such as Ambrose (Reid, Prausnitz and Sherwood, 1987), Constantinou–Gani (Constantinou and Gani, 1994), Lydersen (Reid, Prausnitz and Sherwood, 1987), Joback (Joback and Reid, 1987), and Somayajulu (Somayajulu, 1989) GCMs. The choice of GCMs was more important than the choice of equations of state (EOSs) or mixing rule (MR). Due to most of the accurate solubility prediction obtained from EOSs must include adjustable parameters fitted to experimental data. Accurate critical parameters estimated by GCMs can give more reasonable result in EOSs (Gordillo et al., 2005). Among these GCMs, the easiest ones to use are the Joback and Constantinou–Gani GCMs, which do not require any other GCM to estimate boiling point temperature required for determining critical temperature of solutes, solvent, and cosolvents. The Joback method performs well for low-to-medium molecular weight compounds because experimental data for boiling point temperatures are available. Thus, the estimated value of critical temperature for heavy alkenes and acids by both Constantinou–Gani and Joback GCMs are reasonable accurate. However, experimental data of boiling point temperature are not available for high molecular weight or structurally complex compounds. Therefore, critical properties of those compounds estimated by the Joback method are usually overestimated. If such data are not available, e.g., for heavy compounds, the Constantinou–Gani method should be applied (Žbogar, Da Silva Lopes and Kontogeorgis, 2005). Constantinou et al. gave some emphasis on proper extrapolation of critical properties of high molecular weight compounds. Most very heavy and complex organic compounds have following trend as suggested by Constantinou–Gani GCM. However, the Constantinou–Gani GCM has no structural group parameters needed for some compounds such as carbon dioxide. In this case, the Joback GCM which has more structure group parameters than Constantinou–Gani GCM is used.

In order to test an accuracy of the selected GCM, the critical properties estimated using the Constantinou-Gani GCM was compared with the experimental data. GCM required chemical structure of compounds to predict critical properties. Molecular structures of

substances studied in this work were given in Table 4.1. Table 4.2 shows solid molar volume (V_s) and their average deviations (5.65%) for the solutes. The Aromaticity Index (AI) for the solutes were also presented in Table 4.2. Table 4.3 contained pure component properties of the solutes and solvents studied in this work. The acentric factor (ω) estimated from Lee-Kesler correlation for all substances and the normal boiling point (T_b) for solutes were also included in Table 4.3. The measured properties (Exp.) of solvents and cosolvents (Daubert and Danner, 1990) were compared with the estimates (Est.) predicted using the Constantinou-Gani GCM. The estimates of critical temperature (T_c), pressure (P_c) and volume (V_c) agreed well with the experimental measurements, deviating by an average of 6.23%, 8.71% and 3.85 % for T_c, P_c and V_c respectively. The measured properties of the solutes (Ziger and Eckert, 1983; Haselow et al., 1986; Schmitt and Reid, 1986; Daubert and Danner, 1990; Schultz, Martinelli and Mansoori, 1991; Sakaki, 1992; Poling, Prausnitz and O'Connell, 2001) were compared with the estimated properties by using Constantinou-Gani GCM and tabulated in Table 4.2. The average deviations of T_c, and P_c (Table 4.3) were 6.83% and 16.08%. The average deviation of V_c could not be calculated because no experimental data of V_c for the solutes was available. In summary, the Constantinou-Gani GCM was proven to be suitable for prediction of critical properties of large molecular organic compounds, e.g. cholesterol and β-carotene.

Table 4.1 Molecular structures of substances studied in this work (Daubert and Danner, 1990).

Compounds	Structures	Types of substances
Carbon dioxide	O=C=O	solvent
Acetone	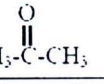	cosolvent
Methanol	CH_3-OH	cosolvent
Ethanol	CH_3-CH_2-OH	cosolvent
Ethane	CH_3-CH_3	cosolvent
Propane	$CH_3-CH_2-CH_3$	cosolvent
n-Butane	$CH_3-CH_2-CH_2-CH_3$	cosolvent
Cyclohexane		cosolvent

Table 4.1 Molecular structures of substances studied in this work (Daubert and Danner, 1990) (con't).

Compounds	Structures	Types of substances
2-napthol	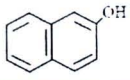	solute
β-carotene	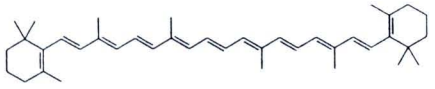	solute
Cholesterol	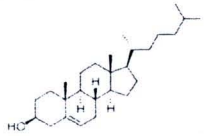	solute
Cholesteryl benzoate	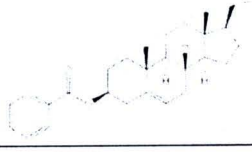	solute
Anthracene	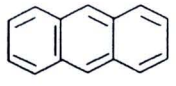	solute
Phenanthrene		solute
Pyrene		solute

Table 4.2 Solid molar volume and aromaticity index of solutes.

Compounds	V_s (cm^3/mol)			$\%\Delta V_s$	AI
	Est.	Exp.	Ref.		
2-Naphthol	134.00	118.46	Schmitt (1986)	13.12	0.29
β-carotene	533.61	536.80	Schultz (1991)	0.59	0.33
Cholesterol	371.69	362.40	Sakaki (1992)	2.56	0.15
Cholesteryl benzoate	450.10	-	-	-	0.25
Anthracene	138.20	142.60	Ziger (1983)	3.09	0.71
Pyrene	144.40	158.50	Ziger (1983)	8.90	0.75
			$\%\Delta V_s$ avg	5.65	

Note: V_s was estimated using Immari and Perini method (Immirzi and Perini, 1977)
AI estimated using Koch method (Koch and Dittmar, 2006)
Est.- Estimated values, Exp.- Experimental values, and Ref.- References

Compound	ω	T_b (K)	T_c (K)			$\%\Delta T_c$	P_c (MPa)			$\%\Delta Pc$	V_c (m^3/kmol)			$\%\Delta Vc$
		Est.	Est.	Exp.	Ref.		Est.	Exp.	Ref.		Est.	Exp.	Ref.	
Solvent and Cosolovents														
Carbon dioxide	0.225	-	304.20	304.12	Daubert (1989)	0.03	7.370	7.374	Daubert (1989)	0.05	0.094	0.094	Daubert (1989)	0.07
Acetone	0.283	-	490.11	508.10	Daubert (1989)	3.54	4.880	4.700	Daubert (1989)	3.84	0.205	0.209	Daubert (1989)	1.91
Methanol	0.506	-	440.91	512.64	Daubert (1989)	13.99	6.509	8.097	Daubert (1989)	19.61	0.110	0.118	Daubert (1989)	6.62
Ethanol	0.556	-	489.28	513.92	Daubert (1989)	4.79	5.557	6.148	Daubert (1989)	9.61	0.165	0.167	Daubert (1989)	1.14
Ethane	0.130	-	363.54	305.32	Daubert (1989)	19.07	4.559	4.872	Daubert (1989)	6.42	0.150	0.146	Daubert (1989)	3.28
Propane	0.172	-	348.49	369.83	Daubert (1989)	5.77	4.547	4.248	Daubert (1989)	7.04	0.201	0.200	Daubert (1989)	0.74
n-Butane	0.215	-	423.12	425.12	Daubert (1989)	0.47	3.988	3.796	Daubert (1989)	5.06	0.257	0.255	Daubert (1989)	0.88
Hexane	0.307	-	516.60	507.60	Daubert (1989)	1.77	3.147	3.025	Daubert (1989)	4.05	0.369	0.368	Daubert (1989)	0.27
Cyclohexane	0.307	-	516.60	553.50	Daubert (1989)	6.67	3.147	4.073	Daubert (1989)	22.73	0.369	0.308	Daubert (1989)	19.73
					$\%\Delta T_c$ avg	6.23			$\%\Delta P_c$ avg	8.71			$\%\Delta V_c$ avg	3.85
Solutes														
2-Naphthol	0.576	541.64	796.70	-	-	-	4.591	-	-	-	0.402	-	-	-
β-carotene	0.486	729.16	898.90	801.00	Schultz (1991)	12.22	5.620	8.090	Schultz (1991)	30.57	2.024	-	-	-
Cholesterol	0.906	656.61	845.38	778.70	Sakaki (1992)	8.56	10.45	12.200	Sakaki (1992)	14.32	1.310	-	-	-
Cholesteryl benzoate	0.769	699.84	892.92	-	-	-	0.866	-	-	-	1.657	-	-	-
Anthracene	0.486	613.4	869.30	869.30	Haselow (1986)	0.00	3.085	2.900	Yaws (1996)	6.37	0.577	0.544	Poling 2001	5.98
Pyrene	0.622	602.25	874.81	936.00	Daubert (1990)	6.54	2.953	2.610	Yaws (1996)	13.13	0.656	-	-	-
					$\%\Delta T_c$ avg	6.83			$\%\Delta P_c$ avg	16.08			$\%\Delta V_c$ avg	-

Notes: ω was calculated using Lee-Kesler correlation (Reid, Prausnitz and Sherwood, 1987)
T_b, T_c, P_c and V_c for all substances except carbon dioxide were estimated using Constantinou-Gani method (Constantinou and Gani, 1994)
For carbon dioxide, T_b, T_c, P_c and V_c were estimated using Joback method (Joback and Reid, 1987)
Est. - Estimated values, Exp. - Experimental values, Ref. - References

4.2 Solubility Modelling

After all critical properties were estimated, fluid–solid phase equilibria using an equation of state approach can be obtained as following in solubility modelling conceptual framework (Figure 4.2).

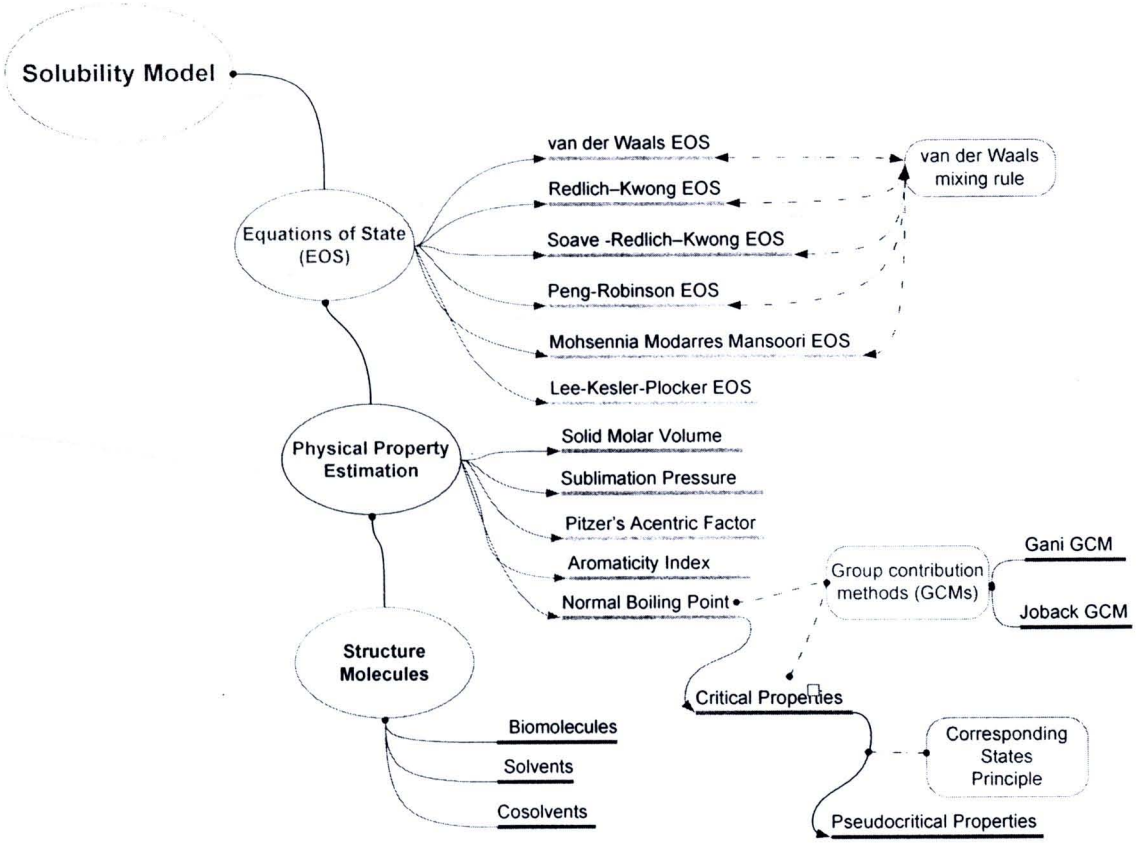

Figure 4.2 Conceptual framework of solubility modelling.

4.2.1 Equations of State Selection

Many cubic equations of state existed in the literatures for modelling fluid–solid equilibrium data were applied. The six EOSs, i.e. van der Waals (vdW), Redlich-Kwong (RK), Soave-Redlich-Kwong (SRK), Peng-Robinson (PR), Mohsen-Nia-Moddaress-Mansoori (MMM) and Lee-Kesler-Plöcker (LKP) EOSs), with the conventional van der Waals mixing rule were used to calculate fugacity coefficients and then solubilities as mentioned before in Chapter 3. In this work, solubilities (y_2*) as a mole fraction of all solute molecules (β-carotene, cholesterol, and cholesteryl benzoate) in $SCCO_2$ with various cosolvent types, mole percent and temperatures (T) were calculated as a function of pressure (P). Binary interaction parameters (k_{ij} and l_{ij}) were assumed to be

zero in all calculations of this work because there was a considerable inconsistency in the experimental data from various sources. It was ascertained that the solubilities obtained from each experiment were independent of supercritical fluid flow rate. All computational programs for modelling were developed in MATLAB (Matrix Laboratory), a powerful symbolic computational language. All programs were tested for several SFE systems published in the literatures (Cygnarowicz, Maxwell and Seider, 1990; Foster et al., 1993; Anitescu and Tavlarides, 1997; Li et al., 2003; Huang, Kawi and Chiew, 2004a). Experimental data for eight systems were collected from the literature (Huang et al., 2004), and fugacity coefficients were predicted with six EOSs (vdW, RK, SRK, PR, MMM and LKP EOSs). To make a reasonable comparison, an average absolute relative deviations (AARD) of predicted values for all systems studied were determined.

The solubility of β-carotene (AI=0.325) in supercritical carbon dioxide with ethanol and methanol as predicted by SRK, vdW, RK, PR, LKP and MMM equations was shown in Figure 4.3 and 4.4. As can be seen from the figures, the solubility increased as pressure increased and most of EOSs (SRK, vdW, PR, and LKP-EOSs) gave accurate prediction except RK and MMM-EOSs. However, SRK, vdW, and PR-EOSs gave overestimated data while LKP-EOS gave more accurate prediction of the solubility of solid solutes in $SCCO_2$ with cosolvents and pressure effects could be represented properly. On the other hand, RK and MMM-EOSs showed wrong direction of solubility prediction trend and gave underestimated results. The error from this numerical method occurred because the estimated values of fugacity coefficients were out of range (0-1).

The solubilities of cholesterol (AI=0.154) in supercritical carbon dioxide with 3 % methanol and acetone at 318.15 and 328.15 K were shown in Figures 4.5-4.8. It was clear on these figures that the MMM equation was much better solubility prediction than the other five equations Similar investigations were performed with cholesteryl benzoate (AI=0.25) and the results were illustrated in Figures 4.9- 4.11. Most of the EOSs (SRK, vdW, PR, and LKP-EOSs) gave right trend of solubility with pressure variation but the values of the solubility were overestimated. On the other hand, RK-EOS could not predict the solubility change with pressure and gave underestimated values of the solubility, as shown in Figure 4.5 and 4.7-4.11.

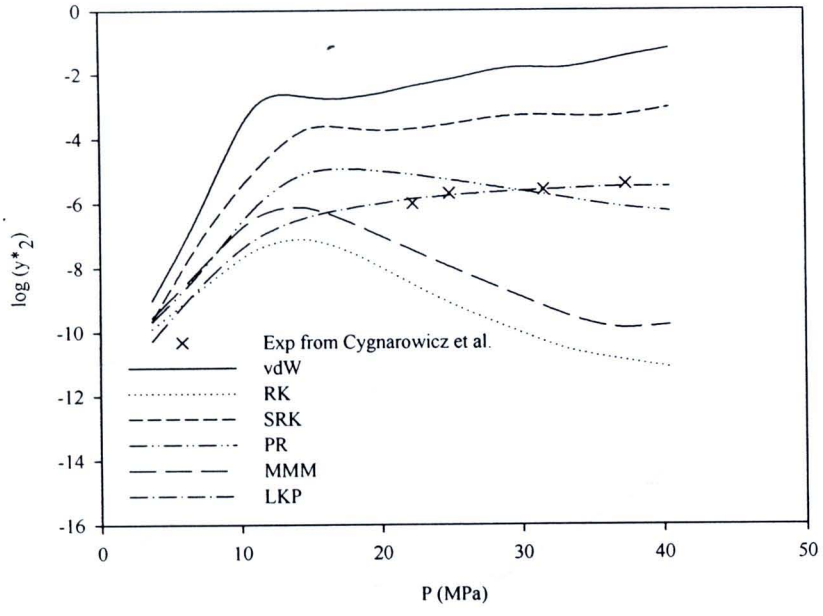

Figure 4.3 β-carotene (AI=0.325) solubility in $SCCO_2$ with 1 wt% ethanol at 343 K.

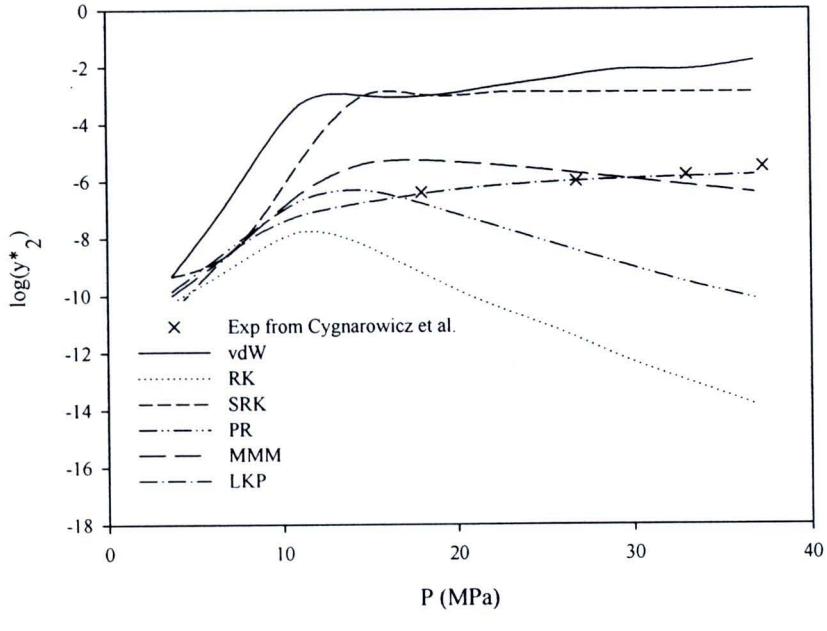

Figure 4.4 β-carotene (AI=0.325) solubility in $SCCO_2$ with 1 wt% methanol at 343 K.

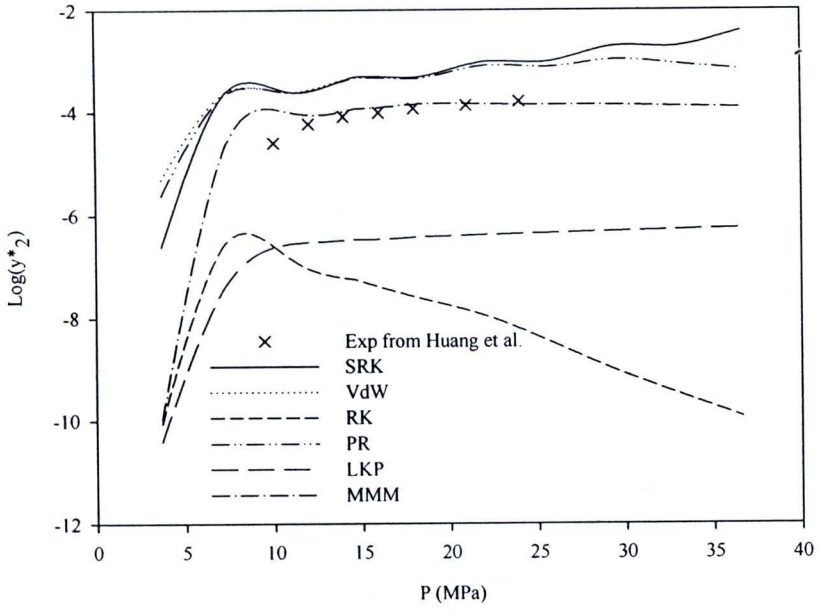

Figure 4.5 Cholesterol (AI=0.154) solubility in $SCCO_2$ with 3 % methanol at 318.15 K.

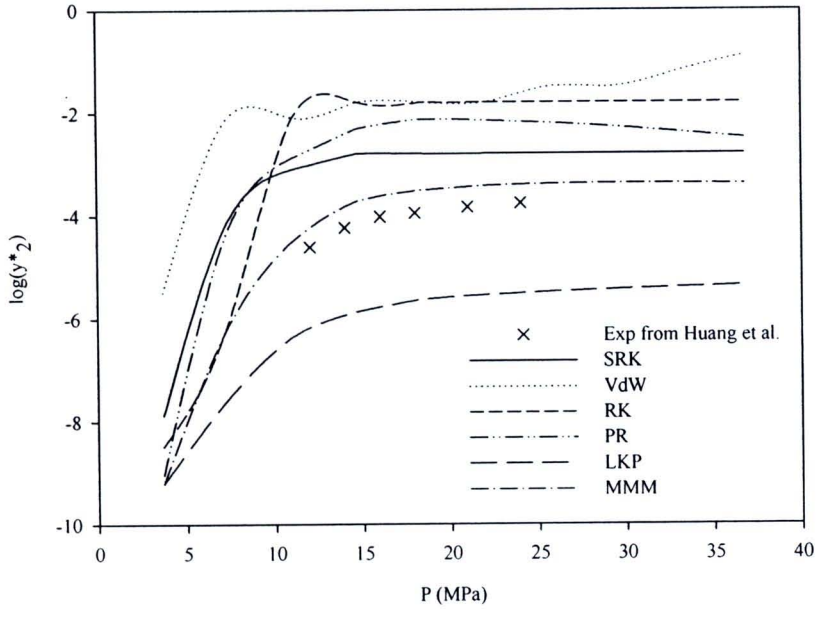

Figure 4.6 Cholesterol (AI=0.154) solubility in $SCCO_2$ with 3 % methanol at 328.15 K.

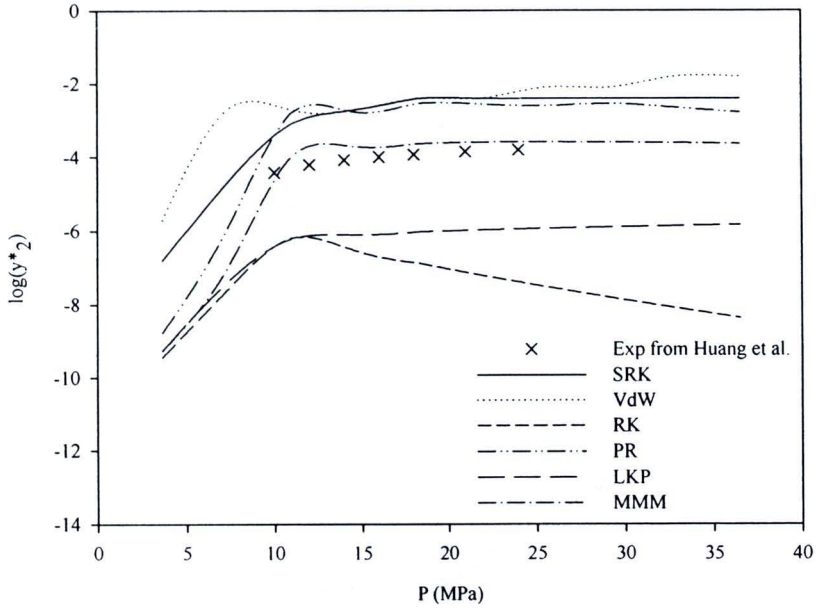

Figure 4.7 Cholesterol (AI=0.154) solubility in $SCCO_2$ with 3 % acetone at 318.15 K.

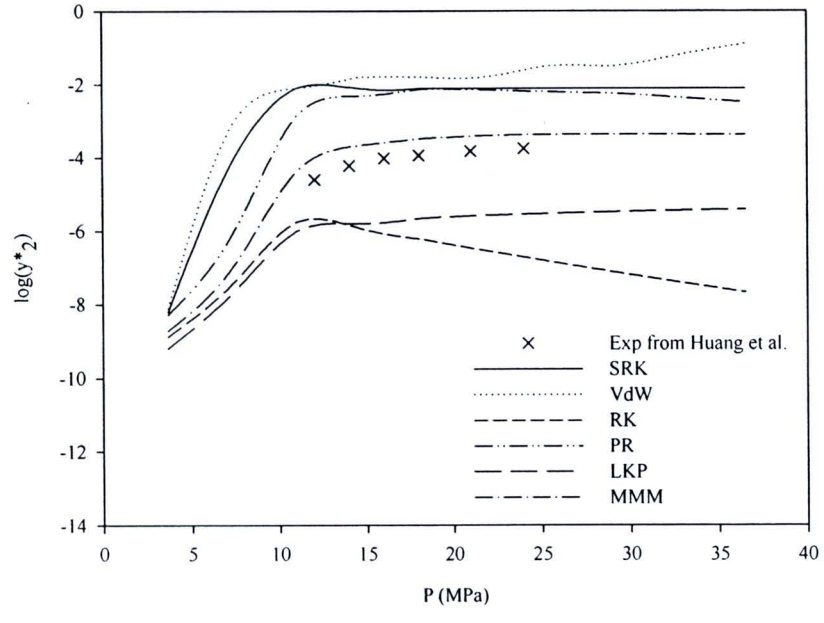

Figure 4.8 Cholesterol (AI=0.154) solubility in $SCCO_2$ with 3 % acetone at 328.15 K.

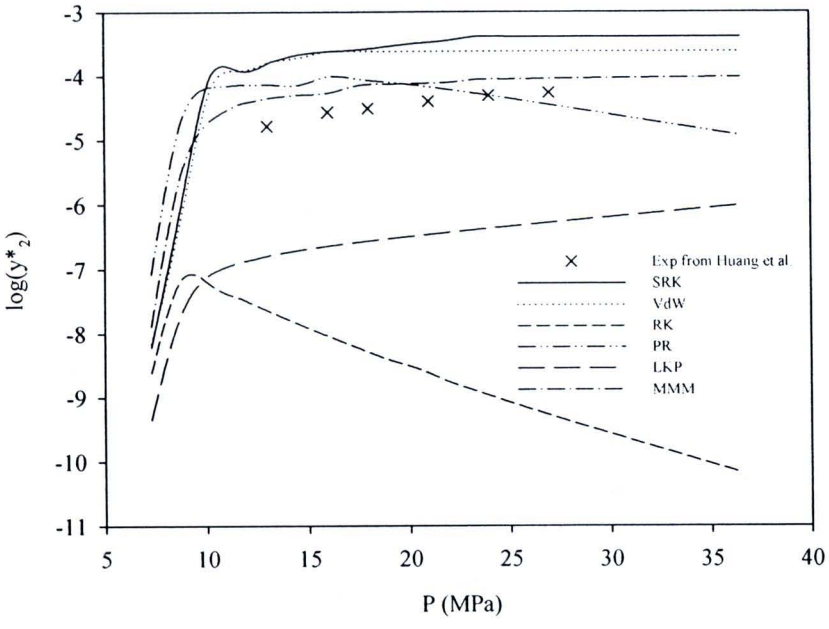

Figure 4.9 Cholesteryl benzoate (AI=0.25) solubility in $SCCO_2$ with 3 % acetone at 318.15 K.

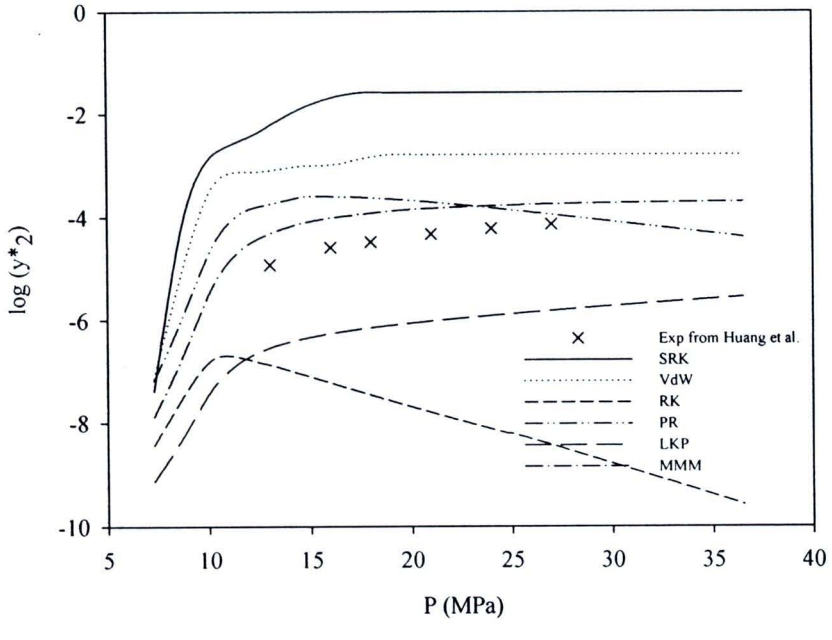

Figure 4.10 Cholesteryl benzoate (AI=0.25) solubility in $SCCO_2$ with 3 % acetone at 328.15 K.

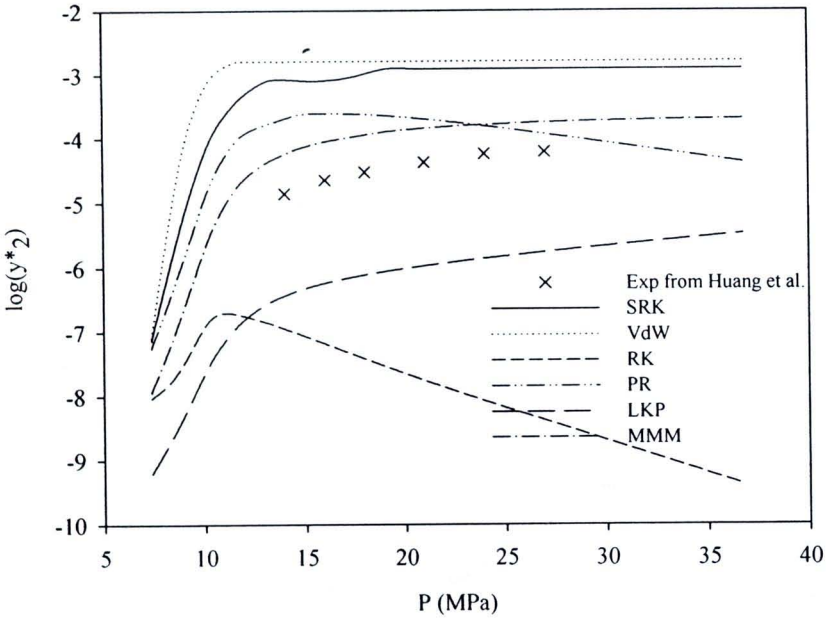

Figure 4.11 Cholesteryl benzoate (AI=0.25) solubility in $SCCO_2$ with 3 % methanol at 328.15 K.

As mentioned before, studied cases were performed with polar cosolvent with pressure or temperature effects. In case of nonpolar cosolvent effect, the solubilities of cholesterol (AI=0.154) in supercritical carbon dioxide with 3.5 % hexane at 318.15, 328.15, and 338.15 K were shown in Figures 4.12-4.14. Again, the MMM EOS gave a better prediction. The effect of cosolvent concentration (3.5 and 6 % hexane) on the cholesterol solubilities was shown in Figures 4.14-4.15. The MMM and LKP EOSs can estimate cholesterol solubility closer than any other EOSs. Even though, all EOSs can present the right trend of solubility variation. MMM-EOS gave a little bit higher predicted value of solubility while LKP-EOS predicted a little bit lower solubility. As can be seen from the figures the LKP and MMM-EOSs should be further studied in more specific to obtain more accurate solubility prediction.

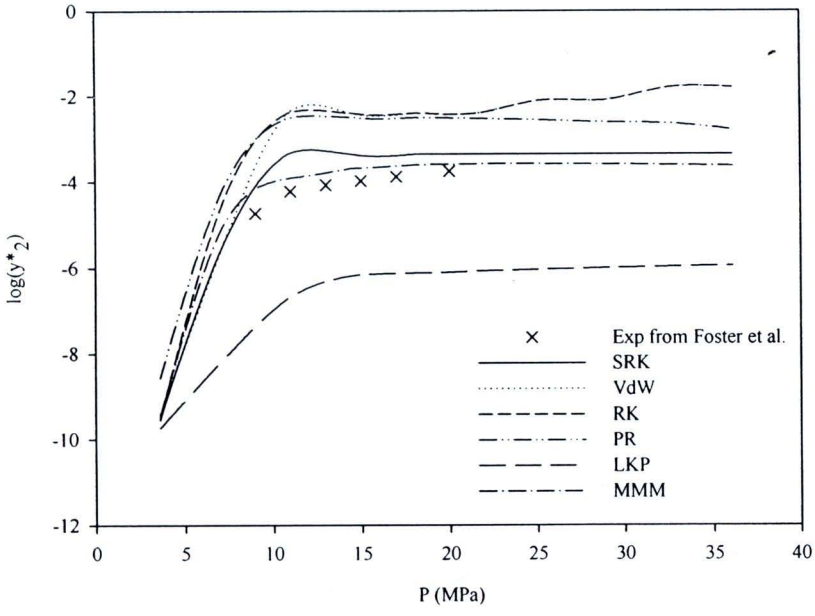

Figure 4.12 Cholesterol (AI=0.154) solubility in $SCCO_2$ with 3.5 % hexane at 318.15 K.

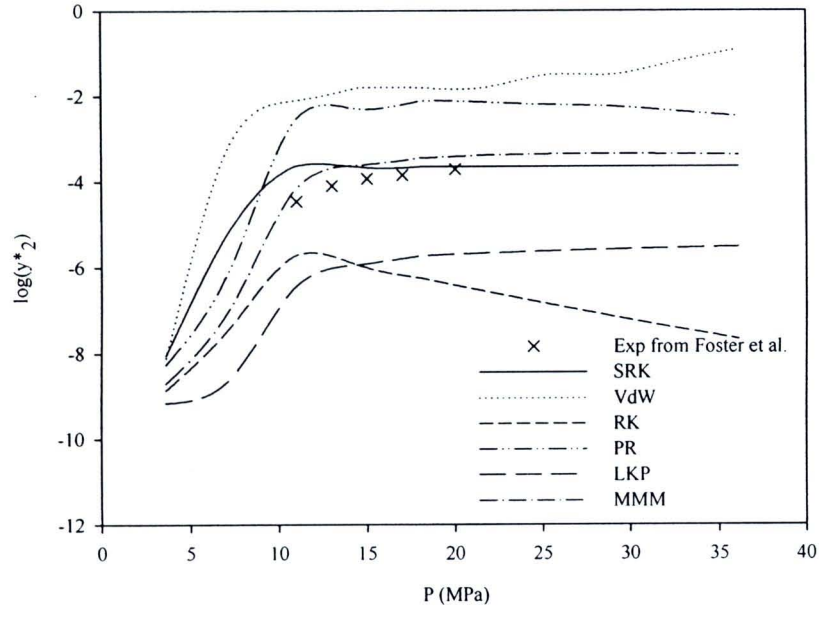

Figure 4.13 Cholesterol (AI=0.154) solubility in $SCCO_2$ with 3.5 % hexane at 328.15 K.

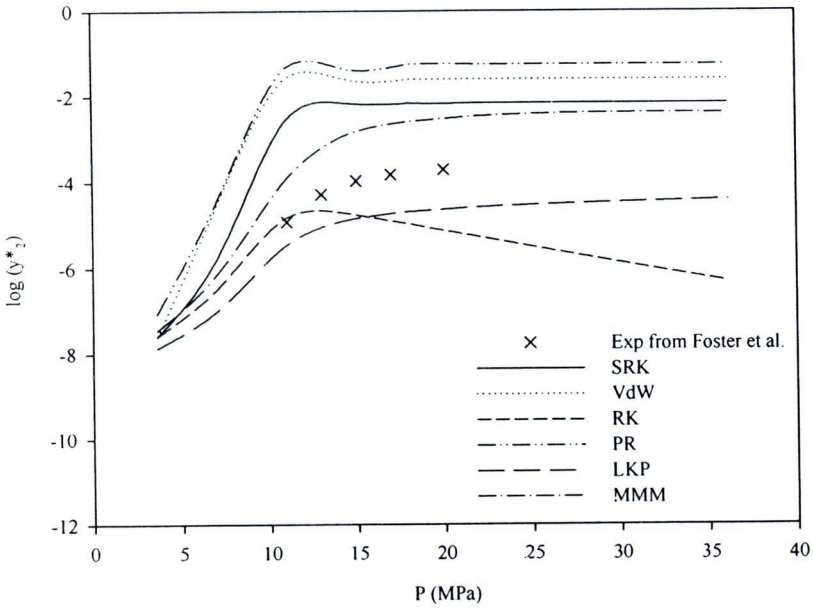

Figure 4.14 Cholesterol (AI=0.154) solubility in $SCCO_2$ with 3.5% hexane at 338.15 K.

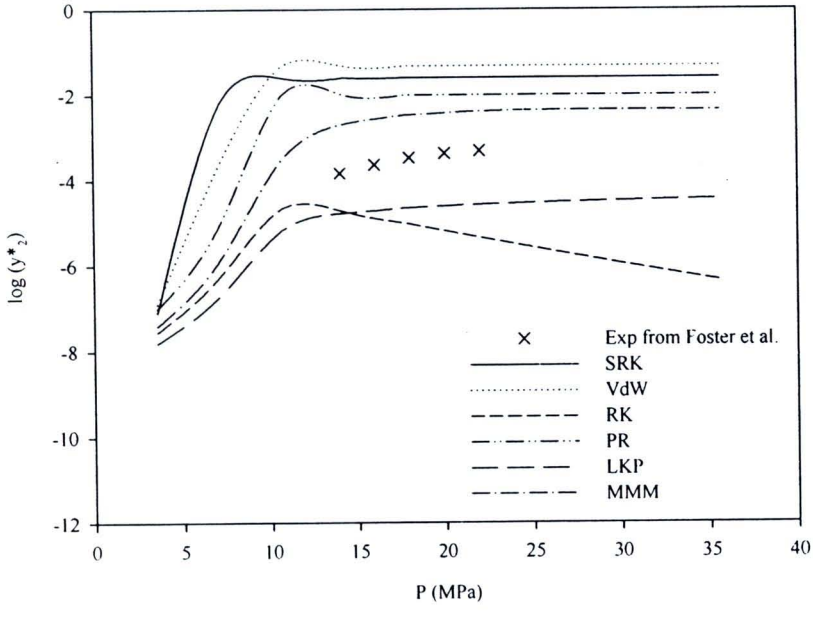

Figure 4.15 Cholesterol (AI=0.154) solubility in $SCCO_2$ with 6% hexane at 338.15 K.

4.2.2 Effects of Critical Properties on the Solubility

The effect of uncertainty of critical properties in solid-gas equilibrium calculations has been investigated for the cholesterol-CO_2-methanol system, using LKP and MMM-EOSs with critical properties from experimental data and Constantinou-Gani GCM. As

depicted in Figure 4.16. The LKP and MMM-EOSs were used to predict the solubility of cholesterol over a range of pressure from 10 to 24 MPa at 318.25 K and 328.25 K. The LKP-Est and MMM-Est curves are the respective LKP and MMM EOS models using critical properties obtained from experiments for the cosolvent (methanol) and the Constantinou-Gani GCM for the solute (cholesterol). The LKP-Gani and MMM-Gani solubility curves applied the Gani GCM to estimate the properties of both the solute and cosolvent. AI for cholesterol (0.154) is less than 0.3, therefore the MMM-EOS should provide the best fit for cholesterol solubility. The results clearly show that the MMM EOS does, in fact, provide a better fit. In addition, there is very little difference between the models using the experimentally measured (-Est) and the estimated (-Gani) properties for the cosolvent (methanol). This result indicated that the errors in estimating the solvent properties (Table 4.2) do not significantly affect the solubility prediction.

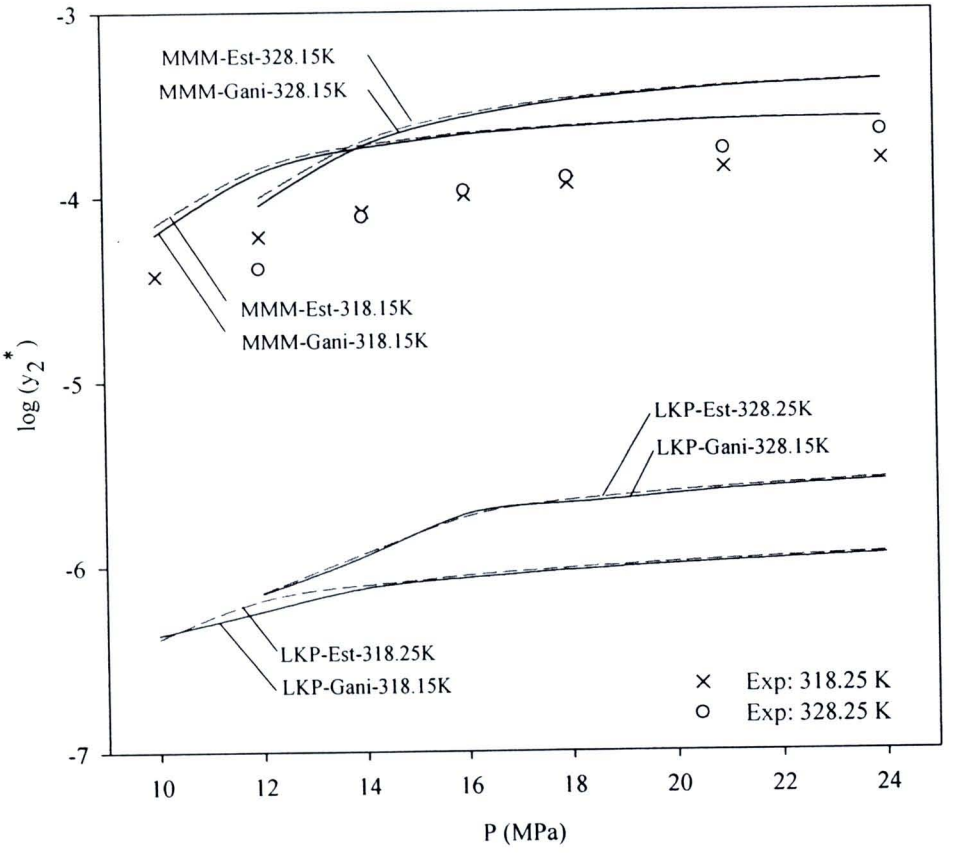

Figure 4.16 Solubility of cholesterol (AI=0.154) in $SCCO_2$ with 3% methanol using physical properties from (-Est): the experiments of Huang et al., 2004b (Huang, Kawi and Chiew, 2004b) and (-Gani): the Constantinou-Gani method.

4.2.3 Solubility of Biomolecules in Supercritical Fluids

Twenty one (21) ternary solute-SCF-cosolvent systems were studied. Tables 4.3-4.6 contained the predicted results of solubilities from 21 ternary systems considered in this work and Figures 4.17-4.24 were plots of several selected cases. (Cygnarowicz, Maxwell and Seider, 1990; Foster et al., 1993; Anitescu and Tavlarides, 1997; Li et al., 2003; Huang, Kawi and Chiew, 2004a) Both polar and nonpolar substances were used as cosolvents. In all cases, the binary interaction parameters between different molecules (k_{ij}) and second interaction parameter (l_{ij}) of the EOSs were set to zero. In addition, the pure component parameters for component i such as energy (a_{ii}) and co-volume parameters (b_{ii}) were calculated from critical properties of pure components which were estimated by group contribution methods. The ternary systems were modelled as quasi binary systems using Kay's mixing rule (Kay, 1936) to estimate the pseudo component properties. The solubility modelling results were presented for four case studies:

4.2.3.1 Polar Solutes with Polar Cosolvents
4.2.3.2 Polar Solutes with Nonpolar Cosolvents
4.2.3.3 Nonpolar Solutes with Polar Cosolvents
4.2.3.4 Nonpolar Solutes with Nonpolar Cosolvents

4.2.3.1 Polar Solutes with Polar Cosolvents

Experimental data for six systems were collected from the literatures (Li et al., 2003; Huang, Kawi and Chiew, 2004a); the solubility results predicted using both the LKP and MMM models were shown in Table 4.3. The AARDs between predicted and experimental values of solubilities for all systems were determined. The AI values for six cases varied from 0 to 0.25; for all six cases the AI was less than 0.3. The average AARD of MMM-EOS estimation was 5.6%. On the other hand, the average AARD of LKP-EOS estimation was 24.7%. Figure 4.17 showed the predicted and measured solubilities of cholesteryl benzoate-CO_2-3% mol methanol system. Since the AI for cholesteryl benzoate was 0.25, the MMM-EOS should again be used and resulted in the AARD of 3.1% and 10.9% at 318.15 K and 328.15 K, respectively. The LKP-EOS gave an AARD of 99.0% and 97.5% at 318.15 K and 328.15 K, respectively Table 4.4.

Table 4.4 Predicted solubility results of polar solid solutes in $SCCO_2$ with polar cosolvents.

Systems (solvent-solute-cosolvent)	cosolvent (% mol)	P (MPa)	T (K)	No. of data points	AI of solute	AARD (%)		References
						LKP	MMM	
CO_2-cholesterol-methanol	3	10.0-24.0	318.15	7	0.154	48.8	2.9	Huang et al. (2004)
			328.15	7		39.4	2.1	
CO_2-cholesterol-acetone	3	10.0-24.0	318.15	7	0.154	50.8	4.8	Huang et al. (2004)
			328.15	7		43.7	4.9	
CO_2-cholesteryl benzoate-methanol	3	13.0-27.0	318.15	6	0.25	99.0	3.1	Huang et al. (2004)
			328.15	6		97.5	10.9	
CO_2-cholesteryl benzoate-acetone	3	13.0-27.0	318.15	6	0.25	36.7	10.8	Huang et al. (2004)
			328.15	6		45.2	6.1	
CO_2-2-naphthol-acetone	3.6	10.05-30	308.1	6	0	38.2	8.7	Li et al. (2003)
			318.1	6		28.8	6.1	
			328.1	6		21.1	5.0	
CO_2-2-naphthol-ethanol	3.6	10.05-30	308.1	6	0	34.3	7.4	Li et al. (2003)
			318.1	6		30.0	8.9	
			328.1	6		24.7	5.6	
Overall AARD (%)						45.6	6.24	

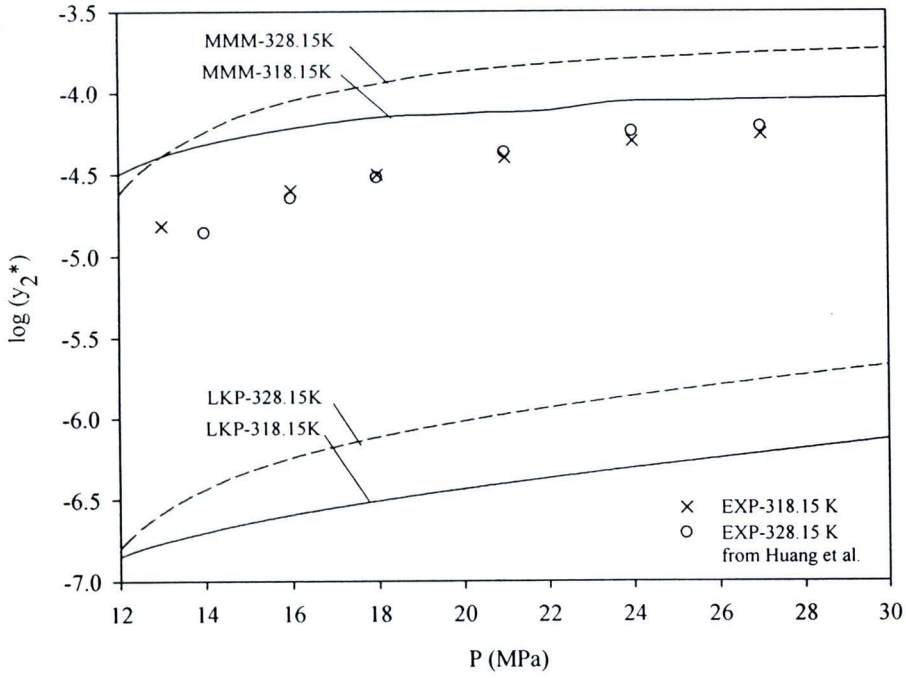

Figure 4.17 Solubility of cholesteryl benzoate (AI=0.25) in $SCCO_2$ with 3% methanol.

4.2.3.2 Polar Solutes with Nonpolar Cosolvents

Experimental solubility data for two polar solutes (cholesterol and 2-napthol) and nonpolar cosolvents (hexane and cyclohexane) systems were collected from the literature (Foster et al., 1993; Li et al., 2003) and presented in Table 4.5. The AIs for the systems of cholesterol and 2-napthol were 0 and 0.154, respectively. Figure 4.18 presented the solubility of 2-naphthol (AI=0) in $SCCO_2$ with 3.6% mol cyclohexane; the MMM-EOS provided a very good fit with the experimental data. The experimental and calculated solubility of 2-naphthol in $SCCO_2$ at 338.1 K with three different cosolvents (acetone, ethanol and cyclohexane) were shown in Figure 4.19. The MMM-EOS provided the best fit with the experimental data using ethanol as a cosolvent, followed by acetone and cyclohexane, respectively. This result was due to types of intermolecular interactions on the polar solute solubility which are mostly dominated by hydrogen bonding, dipole-dipole interaction, and dispersion force for the cases of ethanol, acetone, and cyclohexane, respectively. The overall AARD of MMM and LKP-EOSs for both systems was 11.98% and 49.6%, respectively. This result showed that the MMM-EOS was more appropriate than the LKP-EOS.

Table 4.5 Predicted solubility results of polar solid solutes in CO_2 with nonpolar cosolvents.

Systems (solvent-solute-cosolvent)	cosolvent (% mol)	P (MPa)	T (K)	No. of data points	AI of solute	AARD (%)		References
						LKP	MMM	
CO_2-cholesterol-hexane		9-20	318	6		35.0	10.8	
	3.5	11-20	328	5	0.154	41.8	11.2	Foster, 1993
		11-20	338	5		38.5	9.2	
	6	14-20	338	5		28.2	8.5	
CO_2-2-naphthol-cyclohexane			318.1	6		38.4	8.9	
	3.6	10.05-30	328.1	6	0	34.3	7.5	Li, 2003、
			338.1	6		30.4	7.0	
Overall AARD (%)						49.6	12.0	

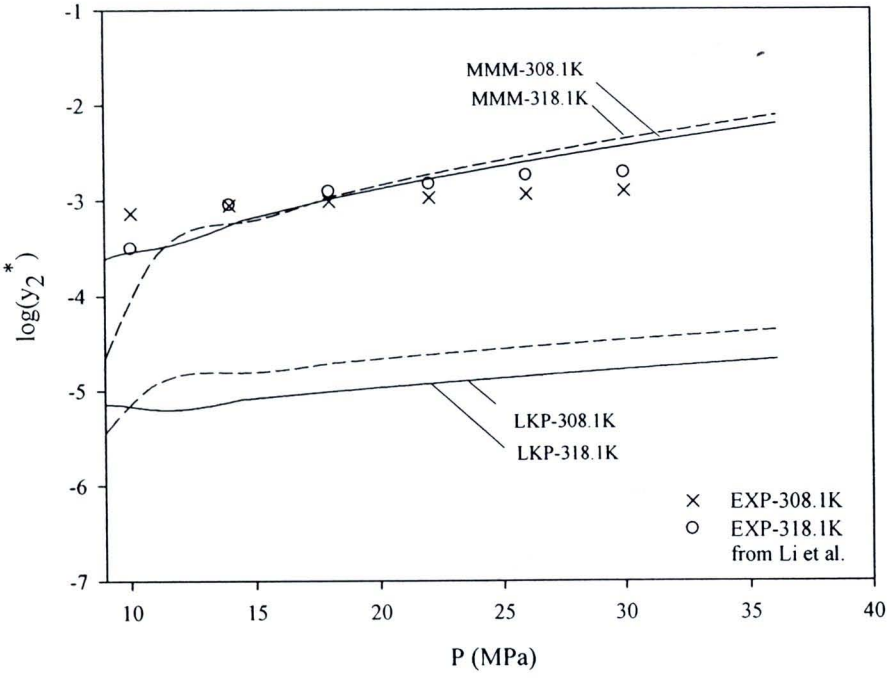

Figure 4.18 Solubility of 2-naphthol (AI=0) in $SCCO_2$ with 3.6% mol cyclohexane.

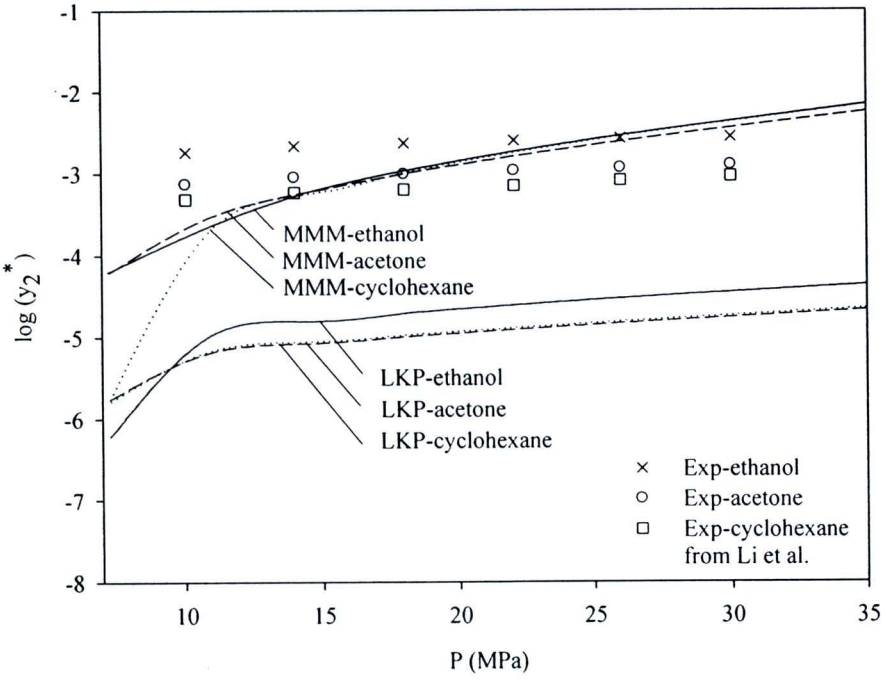

Figure 4.19 The effect of cosolvent types on the solubility of 2-naphthol (AI=0) in $SCCO_2$ with 3.6% mol cosolvent concentration at 338.1 K.

4.2.3.3 Nonpolar Solutes with Polar Cosolvents

Experimental solubility data for six systems were collected from the literatures; (Cygnarowicz, Maxwell and Seider, 1990; Anitescu and Tavlarides, 1997; Li et al., 2003). The results predicted using both the LKP and MMM-EOSs were shown in Table 4.6. It was noticed that AI of nonpolar solutes (pyrene, anthracene, and β-carotene) were higher than 0.3. The solubilities of pyrene (AI=0.75)-CO_2-methanol (5 and 10% mol) systems at 313 and 333 K was shown in Figure 4.20. The solubility of β-carotene (AI = 0.325)-CO_2-1% mol cosolvent concentration (ethanol and methanol) was shown in Figure 4.21. According to these figures and the AI criteria, the LKP-EOS was in good agreement with the experimental solubility data. On the contrary, the MMM-EOS predicted solubility values lower than the experimental data. In addition, the MMM-EOS gave wrong trend of solubility with respect to pressure variation compared with the experimental data. At higher pressure, the solubilities of β-carotene-CO_2 ethanol and methanol predicted using the MMM-EOS decreased (Figure 4.21). These wrong trend of solubility variations of biomolecules in $SCCO_2$, predicted from various EOSs, also occurred in other literatures (Hartono, Mansoori and Suwono, 2001). As shown in Table 4.6, the average error of the LKP and MMM-EOSs were 8.5% and 76.8%, respectively. This confirmed that the LKP-EOS was preferred much more than the MMM-EOS for solubility prediction of nonpolar solutes-polar cosolvent systems.

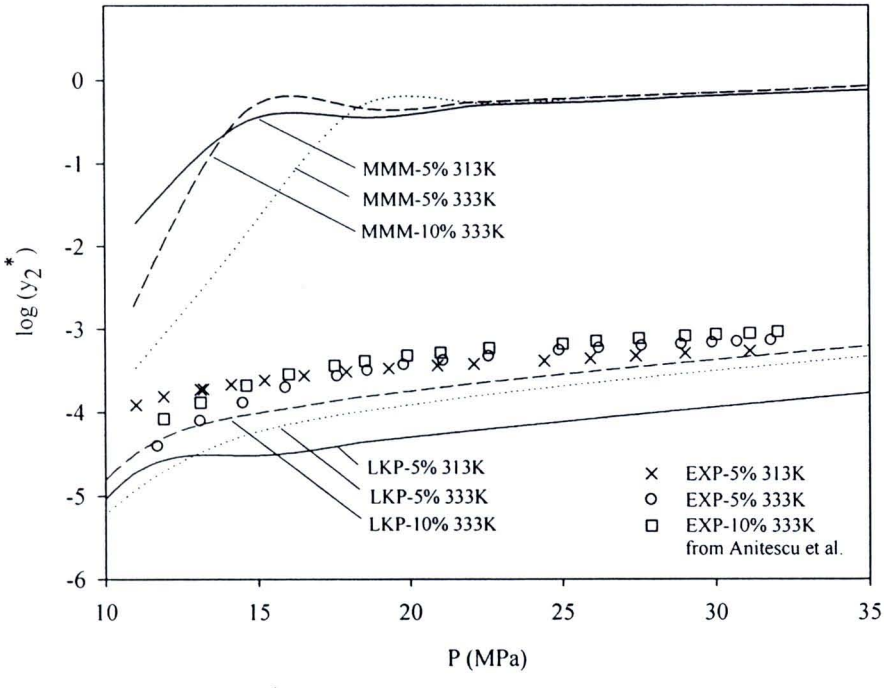

Figure 4.20 The effects of temperature and methanol concentration on the solubility of pyrene (AI=0.75) in $SCCO_2$.

Table 4.6 Predicted solubility results of nonpolar solid solutes in $SCCO_2$ with polar cosolvents.

Systems (solvent-solute-cosolvent)	cosolvent (% mol)	P (MPa)	T (K)	No. of data points	AI of solute	AARD (%)		References
						LKP	MMM	
CO_2-pyrene-methanol	5	11.0-31.1	313	16		21.0	81.9	
		11.7-31.8	333	16	0.75	10.2	79.2	Anitescu, 1997
	10	11.9-32.0	333	16		9.3	78.7	
CO_2-anthracene-ethanol			308.1	5		2.7	92.5	
	4	10.0-30.0	318.1	5	0.71	6.7	90.4	Li, 2003
			328.1	5		10.0	86.6	
CO_2-anthracene-methanol	5	13.8-30.7	313	13		7.1	93.8	
		13.7-30.0	333	13	0.71	12.6	93.7	Anitescu, 1997
	10	13.9-30.7	333	13		14.2	94.0	
CO_2-anthracene-acetone			308.1	5		4.6	92.7	
	4	10.0-30.0	318.1	5	0.71	7.6	88.2	Li, 2003
			328.1	5		10.6	82.3	
CO_2-β-carotene-ethanol	1 wt%	22.3-37.4	343	4	0.325	1.2	9.6	Cygnarowicz, 1990
CO_2-β-carotene-methanol	1 wt%	18.0-37.3	343	4	0.325	0.5	11.4	Cygnarowicz, 1990
Overall AARD %						8.5	76.8	

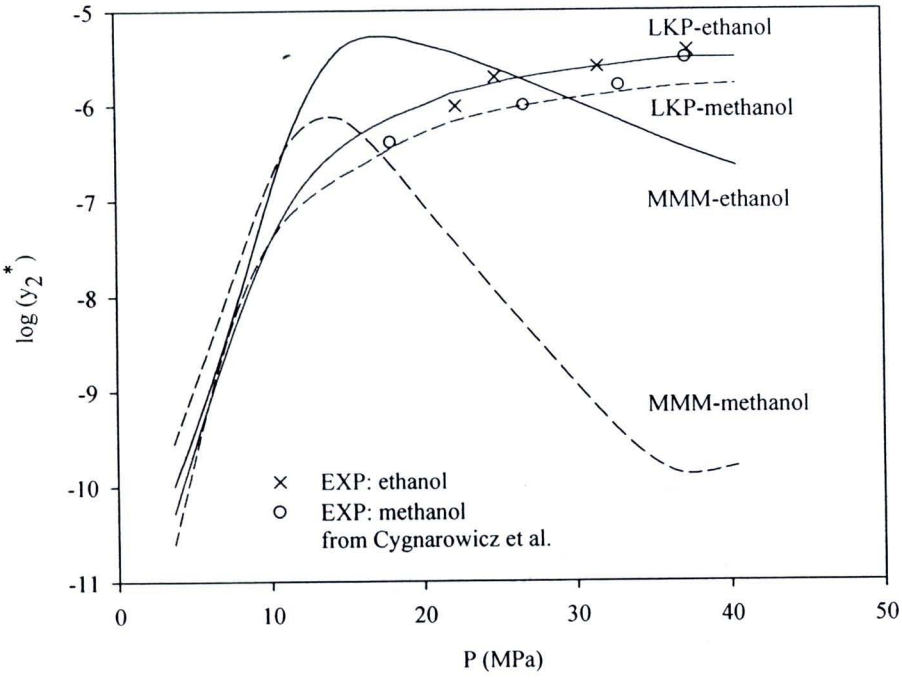

Figure 4.21 The effect of cosolvent type on the solubility of β-carotene (AI=0.325) in $SCCO_2$ with 1% mol cosolvent at 343 K.

4.2.3.4 Nonpolar Solutes with Nonpolar Cosolvents

Experimental solubility data for seven systems were collected from the literatures, (Anitescu and Tavlarides, 1997; Li et al., 2003) and the predicted solubility results using both the LKP-EOS and MMM-EOS were shown in Table 4.7. Figure 4.22 shows the comparison between the predicted and measured solubilities for the pyrene (AI=0.75)-CO_2-butane (5 and 10 % mol) systems at 313 and 333 K. Figure 4.23 illustrates the effect of cosolvent types on the solubility of anthracene (AI=0.71) in carbon dioxide at 308.1 K. As can be seen from the figures, cyclohexane enhanced CO_2 dissolution in nonpolar solutes better than ethanol and acetone. This may be attributed to the interactions between the solute and cosolvent molecules of this system depended mainly on the dispersion force. The average error of LKP-EOS and MMM-EOS were 13.0% and 85.8%. In both cases the LKP-EOS performed a better fit than the MMM-EOS when solutes were nonpolar. To ensure that our proposed methodology correctly model the solubility of biomolecules in supercritical fluids system, Figure 4.24 was a summary of the AARDs between the measured and predicted solubilities of all 62 cases from the 21 systems presented in Tables 4.4-4.7. AARD (AI^+) was the designation for AARD obtained from the predicted results using the EOS selected based on the so-called AI

criteria (i.e. if AI $\leq$ 0.3 use the MMM EOS and if AI > 0.3 use the LKP EOS (Ajchariyapagorn et al., 2008)) whereas AARD (AI^-) was the designation for the AARD obtained when one did not follow the AI criteria. When the AI criterion was used, the average AARD (AI^+) ranged from 0.5% to 25.5% with an average of 10.0% otherwise the AARD (AI^-) ranged from 9.6% to 99% with an average of 69.0% (Table 4.8). The results clearly showed the importance of the AI criteria for solubility prediction.

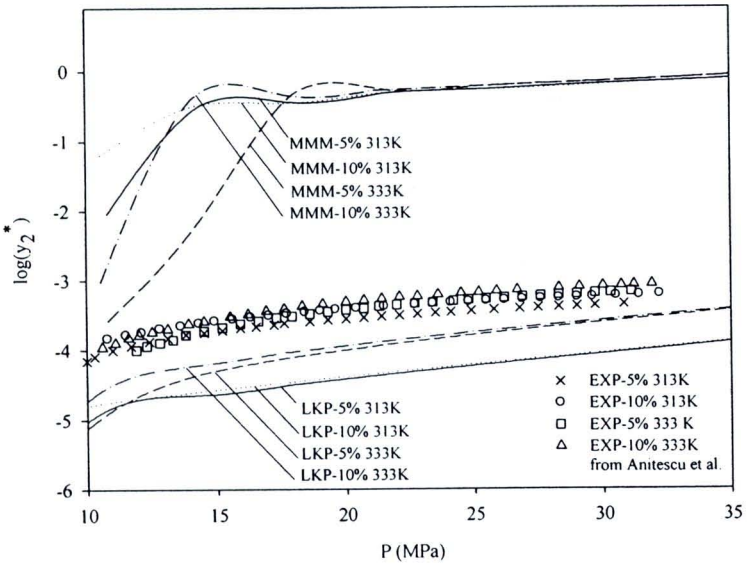

Figure 4.22 The effect of butane concentration on the solubility of pyrene (AI=0.75) in $SCCO_2$.

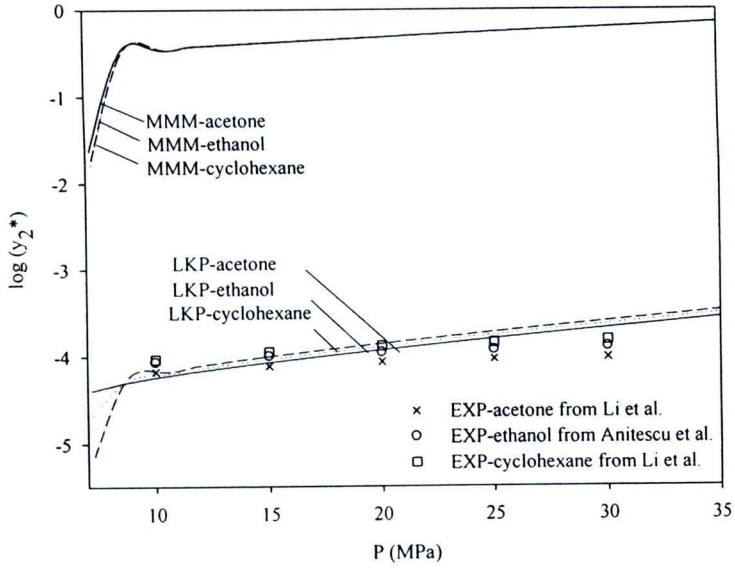

Figure 4.23 The effect of cosolvent types on the solubility of anthracene (AI=0.71) in $SCCO_2$ with 4% mol cosolvent concentration at 308.1 K.

Table 4.7 Predicted solubility results of nonpolar solid solutes in $SCCO_2$ with nonpolar cosolvents.

Systems (solvent-solute-cosolvent)	cosolvent (% mol)	P (MPa)	T (K)	No. of data points	AI of solute	AARD (%)		References
						LKP	MMM	
CO_2-pyrene-ethane	5	11.1-34.4	313	30	0.75	16.9	85.5	Anitescu, 1997
		11.0-34.0	333	30		23.3	77.0	
	10	11.0-34.0	313	30		11.7	87.7	
		11.1-33.1	333	30		12.6	81.5	
CO_2-pyrene-propane	5	10.8-31.1	313	30	0.75	23.1	84.2	Anitescu, 1997
		10.7-31.7	333	30		25.5	84.2	
	10	11.0-31.3	313	30		15.9	80.6	
		10.2-31.5	333	30		18.8	59.4	
CO_2-pyrene-butane	5	10.0-30.8	313	30	0.75	22.6	84.0	Anitescu, 1997
		11.9-31.1	333	30		15.3	76.5	
	10	10.8-32.2	313	30		25.0	87.6	
		10.6-31.9	333	30		16.1	82.3	
CO_2-anthracene-ethane	5	10.8-35.0	313	28	0.71	8.9	90.9	Anitescu, 1997
		11.0-35.0	333	28		12.5	90.5	
	10	10.7-35.0	313	28		8.2	92.9	
		12.0-35.0	333	28		13.4	89.6	
CO_2-anthracene-propane	5	12.0-36.6	313	27	0.71	8.0	92.8	Anitescu, 1997
		11.6-35.0	333	30		9.3	88.0	
	10	10.7-35.1	313	28		6.1	92.4	
		11.6-35.0	333	30		8.7	86.8	
CO_2-anthracene-butane	5	12.0-36.6	313	26	0.71	7.9	92.7	Anitescu, 1997
		11.6-35.0	333	26		9.7	85.4	
	10	10.7-35.1	313	26		9.2	91.8	
		11.6-35.0	333	26		8.7	89.0	
CO_2-anthracene-cyclohexane	4	10.0-30.0	308.1	5	0.71	1.6	91.0	Li, 2003
		10.0-30.0	318.1	5		4.5	92.0	
		10.0-30.0	328.1	5		7.7	80.6	
Overall AARD %						13.0	85.8	

Table 4.8 AARD % for all predicted solubility results based on AI criterion.

Systems		Average AARD %		AARD % range			
				LKP-EOS		MMM-EOS	
Solute type	Cosolvent type	LKP-EOS	MMM-EOS	Min.	Max.	Min.	Max.
Polar	Polar	45.6	6.24	2.1	*99.0*	2.1	10.9
	Nonpolar	49.6	11.98	28.2	41.8	7.0	11.2
Nonpolar	Polar	8.5	76.8	0.5	21.0	*9.6*	94.0
	Nonpolar	13	85.8	1.6	25.5	59.4	92.9
			AI^+	0.5	25.5	Avg. AI^+	10
			AI^-	9.6	99.0	Avg. AI^-	69

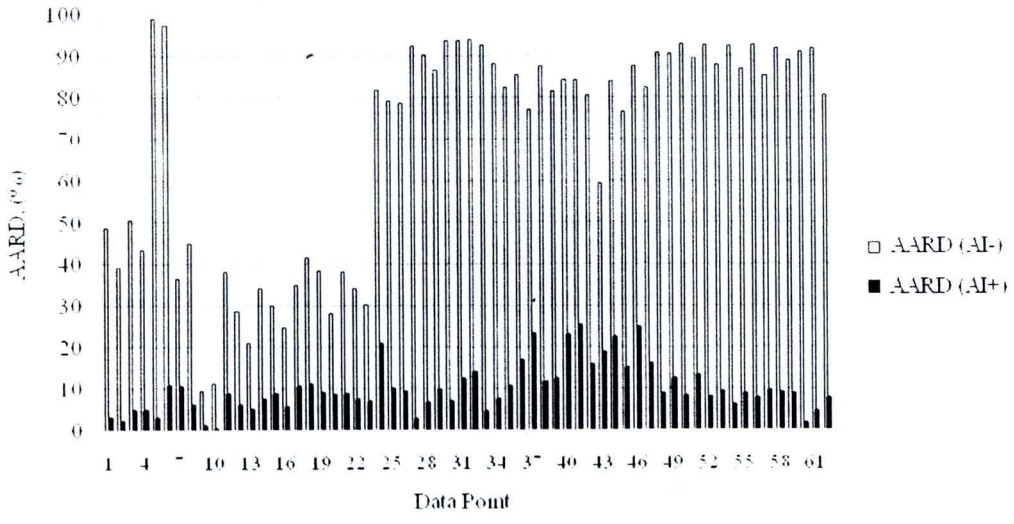

Figure 4.24 AARD (AI^+) and AARD (AI^-) for each data point in Tables 4.3-4.6.

4.3 Supercritical Fluids Extraction Modelling Results

The theoretical model developed was tested after the phase equilibrium between fluid and solid (solubility) could be obtained from section 4.2. In order to validate the models, comparisons with measured yield were verified without adjusted parameters. The extraction curves were determined in which the following parameters were varied: pressure, temperature, CO_2 flow rate, particle size, and cosolvent concentration (section 4.3.1). Moreover, our investigation involved the parametric studies (section 4.3.2). The model parameters were disturbed to see how transport parameters affected the model. From these results, it is possible to propose strategies for high performance operation by extractor configuration (section 4.3.3).

The procedure of process simulation (Figure 4.25) consists of the resolution of the set of mathematical relations that describe system behaviour with 3 parts: (1) properties estimations, (2) solubility estimation, and (3) extraction estimation. The mathematical model requires input variables such as the molecular structure of solute, solvent and co-solvent and operating conditions (temperature, pressure, particle size, solvent flow rate, bed length, column diameter, and raw material weight).

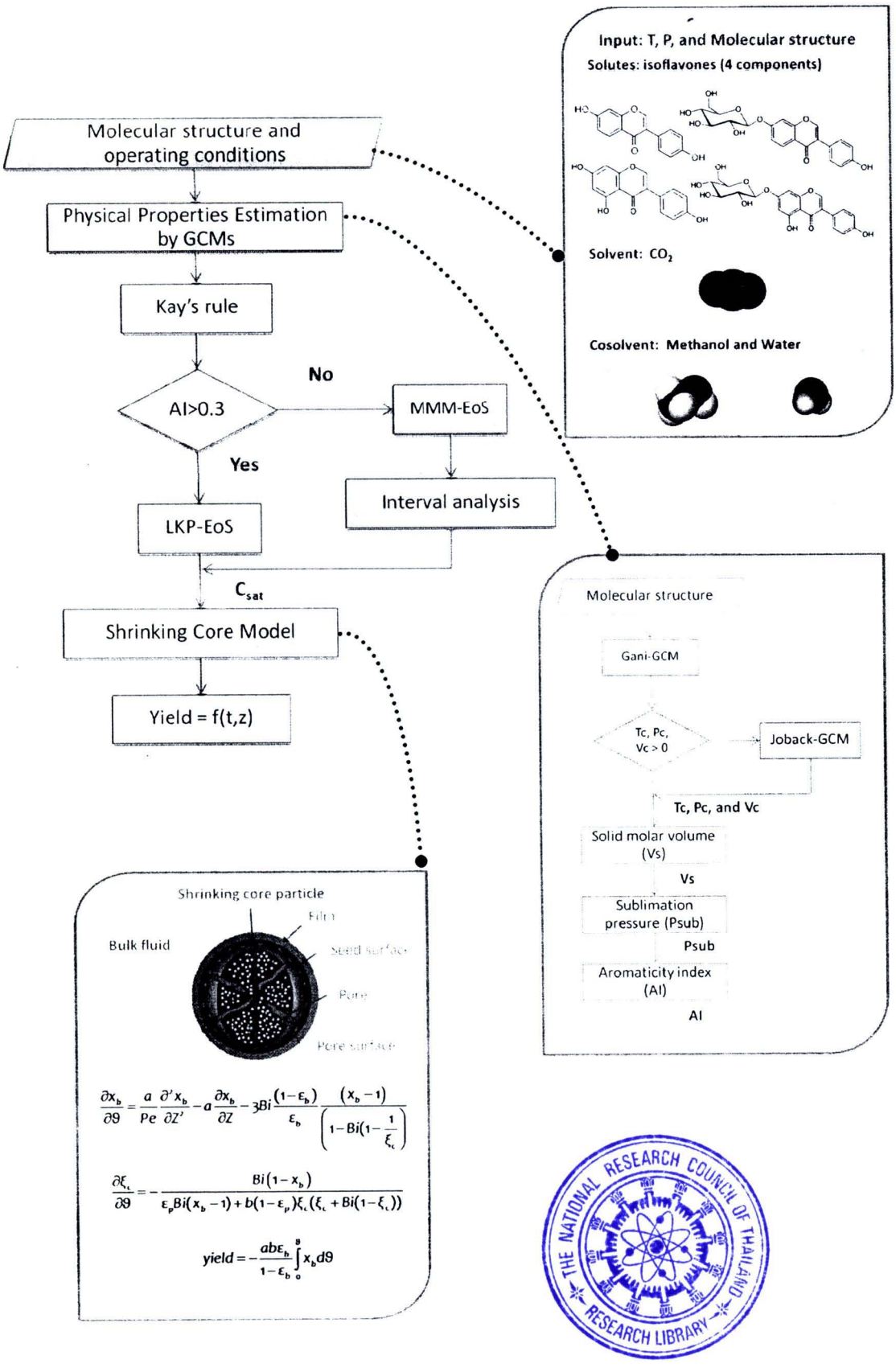

Figure 4.25 Summary of all methodologies used in this research.

Before performing the simulation, first it is important to check the validation of model assumptions. The developed model was validated with Zuo et al.'s data (Zuo et al., 2008). It was multicomponent solute system as depicted in Table 4.9. As previously mentioned, the pseudo-component assumption was introduced to simplify the prediction of phase equilibrium. This assumption was supported by some recent researches dealing with the isoflavone extraction (Rostagno, Araújo and Sandi, 2002; Araújo, Silva and Chaves, 2007). These works demonstrated that the compositions remained the same at various conditions. Even though the mole fraction of isoflavones obtained from these two sources are different due to the preparation method used. Each composition of both cases remains the same for every condition (Figure 4.26). This is reasonable to apply with Zuo et al.'s data (Zuo et al., 2008). Daizin is the major component in soybeans (55 wt% or 46 mol% of total isoflavones) hence the physical properties of soy isoflavones depend mainly on this component. The MMM-EOS was preferred to estimate the solubility because of daizin's aromaticity index value (AI = 0.1).

Table 4.9 Parameters and characteristics of isoflavone extraction process (Zuo et al., 2008).

Characteristics of the raw material			*Operating conditions*		
mean particle size	3.5×10^{-6}	m	Soybean meal weight	100	g
total isoflavones	2,628.4 ± 51.6	μg/g	$SCCO_2$ flow rate	5.88	kg/h
Daidzin	1,445.9 ± 48.4	μg/g	Modifier flow rate	0.6	L/h
Daidzein	459.8 ± 39.3	μg/g	Temperature	40	°C
Genistin	326.5 ± 25.8	μg/g	Pressure	50	MPa
Genistein	396.1 ± 10.2	μg/g	Extraction time	210	min
Solvent-cosolvent concentration			*Characteristics of the extractor*		
Carbon dioxide	92.2	wt %	Length	0.725	m
Methanol and water	7.8	wt %	Diameter	0.042	m
(80:20, v/v)			Volume	1	L

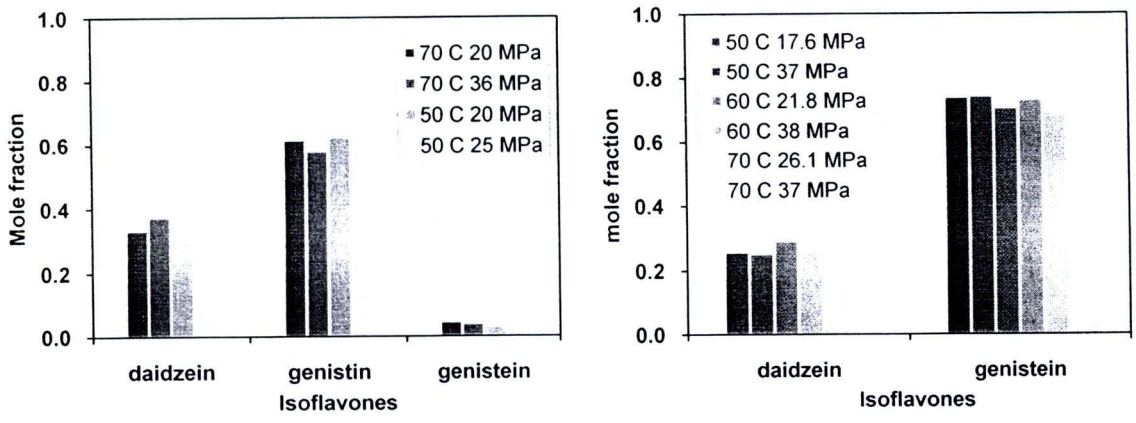

Figure 4.26 Compositions of isoflavones extracted from soybeans at various temperatures and pressures using 10 mol% of cosolvent (a) 70% aqueous methanol (Araújo, Silva and Chaves, 2007) and (b) 80% aqueous methanol (Rostagno, Araújo and Sandi, 2002).

4.3.1 Model Validation: Effect of operating parameters on supercritical extraction yield

To validate the model, we used the data published by Zuo et al. (Zuo et al., 2008) for $SCCO_2$ extraction of soybeans. The operating conditions, characteristics of the raw material and extractor and the compositions of solvents and modifiers required for the model were presented in Table 4.9. In order to analyze the effect of the operating parameters (pressure, temperature, CO_2 flow rate, particle size, and cosolvent concentration) on extraction process, the extraction yields expressed as grams of extract/ 100 g of dry soybeans for an extraction time of 210 min were used under different conditions. Pilot plant scale of the extractor (a pressurized vessel of 1 L (L/D = 20)) has been employed. The extracts were described as a single pseudo-component in this model for their similar behaviour with respect to the mass transfer phenomena (Özkal, Yener and Bayındırlı, 2005; Machmudah et al., 2006). Once structural molecule of all substances was obtained (Table 4.10), the physical properties could be estimated as shown in Tables 4.11. All estimated transport properties for each process condition were presented in Table 4.12. Figure 4.27 showed the variation of extraction yield as a function of axial distance along the bed and time of Run No. 3 in Table 4.13. This run was chosen as a reference case in the sensitivity analysis part (section 4.3.2).

Table 4.10 Molecular structure of isoflavones studied (Daubert and Danner, 1990).

Compound	Structure	Type of Substance
diadzin	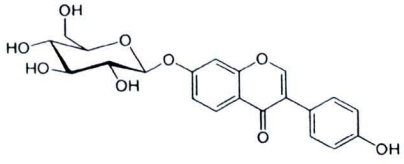	solute
daizein	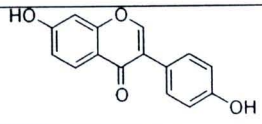	solute
genistin	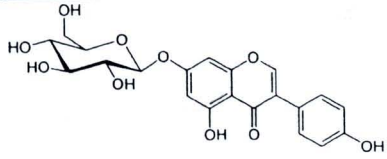	solute
genistein	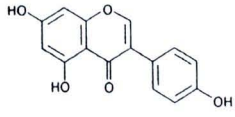	solute

Table 4.11 Physical properties of solutes and solvents.

Compound	*Formula*	*MW*	*ω*	T_b *(K)*	T_c *(K)*	P_c *(MPa)*	V_c *(m^3/kmol)*	v_s *(m^3/kmol)*	*AI*
Carbon dioxide	CO_2	44.00	0.23	-	304.200	7.370	0.094	-	-
Methanol	CH_3OH	32.04	0.51	-	440.911	6.509	0.110	-	-
Water	H_2O	18.00	0.35	-	647.096	22.064	0.056	-	-
Daidzin	$C_{21}H_{20}O_9$	416.4	1.638	1,357.37	1,699.15	3.076	0.970	0.460	0.1
Daidzein	$C_{15}H_{10}O_4$	254.2	1.476	786.77	1,168.69	4.578	0.556	0.326	0.6
Genistin	$C_{21}H_{20}O_{10}$	432.4	1.657	1,456.45	1,847.15	3.995	0.925	0.492	0.0
Genistein	$C_{15}H_{10}O_5$	270.2	1.604	957.39	1,242.28	5.662	0.521	0.298	0.56

Where *MW*: molecular weight, ω: acentric factor, T_b: normal boiling point temperature, T_c: critical temperature, P_c: critical pressure, V_c: critical volume, v_s: solid molar volume, and *AI*: aromaticity index.
Note: The estimated properties were calculated using Ajchariyapagorn et al. method (Ajchariyapagorn et al., 2008).

Table 4.12 Process parameters obtained for the supercritical extraction of isoflavones from soybean meal (Zuo et al., 2008).

Run no.	Operating conditions					C_{sat}	ρ_m	μ_m	Bi	Re	Sc	Sh	Pe	k_f	D_{AB}	D_e	D_L
	P	T	Q	d_p	CS		($\times10^{-2}$)	($\times10^{4}$)						($\times10^{5}$)	($\times10^{9}$)	($\times10^{9}$)	($\times10^{5}$)
	(MPa)	(°C)	(kg/h)	(mm)	(wt %)	(g/g)	(kg/m^3)	(kg/(m.s))						(m/s)	(m^2/s)	(m^2/s)	(m^2/s)
1	30	40	5.88	0.68	7.8	0.0686	8.828	1.976	1.82	6.10	26.98	5.04	131.15	6.152	8.297	11.480	1.175
2	40					0.0760	9.337	2.212	1.83	5.74	31.30	5.74	131.94	5.052	7.568	10.480	1.210
3	50					0.0852	9.745	2.491	1.80	5.32	36.21	4.98	133.07	5.166	7.060	9.773	1.244
4	60					0.0918	10.087	2.718	1.78	5.05	40.40	4.94	133.90	4.844	6.670	9.233	1.273
5	50	50	5.88	0.68	7.8	0.0860	9.401	2.249	1.77	5.40	33.10	4.89	132.84	5.472	7.607	10.530	1.208
6		60				0.0869	9.062	2.256	1.73	5.466	30.37	4.8	132.67	5.786	8.197	11.350	1.174
7		70				0.0881	8.730	2.159	1.70	5.50	28.00	4.70	132.57	6.103	8.833	12.230	1.140
8	50	40	3.92	0.68	7.8	0.0852	9.745	2.491	1.28	3.53	36.21	3.53	140.92	3.668	7.060	9.773	0.703
9			7.84			0.0852	9.745	2.491	2.27	7.04	36.21	6.28	129.30	6.519	7.060	9.773	1.838
10			9.80			0.0852	9.745	2.491	2.73	8.81	36.21	7.56	126.97	7.846	7.060	9.773	2.511
11	50	40	5.88	0.48	7.8	0.0852	9.745	2.491	2.90	3.54	36.21	3.55	199.49	5.219	7.060	4.319	0.723
12				1.19		0.0852	9.745	2.491	3.36	7.52	36.21	6.63	58.99	3.934	7.060	6.958	2.191
13	50	40	5.88	0.68	5.4	0.0813	9.756	2.407	1.82	5.51	34.19	5.03	132.53	5.337	7.218	9.991	1.233
14					10.2	0.0894	9.729	2.582	1.78	5.13	38.46	4.92	133.66	4.994	6.902	9.554	1.258

Note: **Operating conditions** T: temperature, P : pressure, Q: volumetric flow rate, d_p: particle size, CS: cosolvent concentration
Dimensionless Bi: Biot number, Re: Reynolds number Sc: Schmidt number, Sh: Sherwood number, Pe: Peclet number
Transport properties C_{sat}: saturated solute concentration in $SCCO_2$, ρ_m: mixture density, μ_m: mixture viscosity, k_f: film mass transfer coefficient, D_{AB}: diffusion coefficient of solutes (A) in supercritical solvents (B), D_e: effective diffusivity, and D_L: axial dispersion coefficient

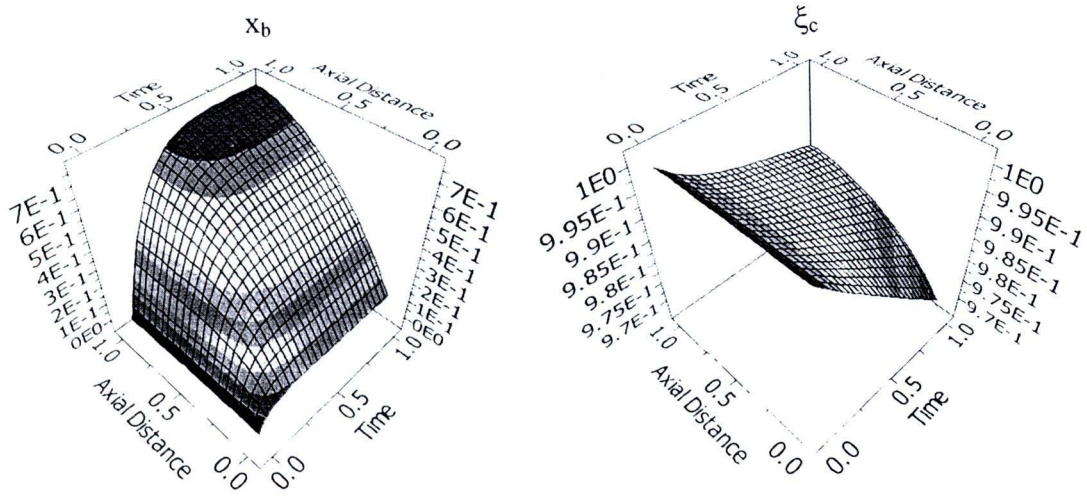

(a) (b)

Figure 4.27 Response surface plot of Run no. 3 (in Table 4.9) showing (a) the effect of axial distance along the fixed bed and time on the extracted isoflavones and (b) core radius of soybean.

4.3.1.1 Effect of Pressure

Figure 4.28 shows the effect of pressure on the extraction profile. As can be seen, the maximum yield obtained at the highest pressure. Extraction profiles, in terms of the experimental data points and the model prediction (continuous line), were generally composed of a nearly linear initial portion (fast extraction period) and a flat end tail (slow extraction period) connected by a transition section zone.

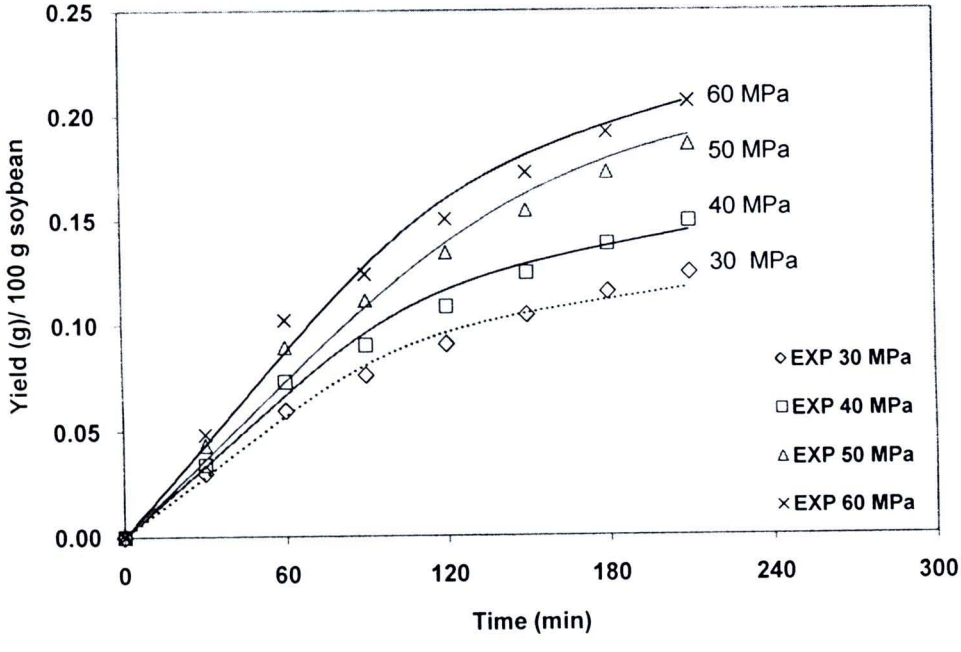

Figure 4.28 Pressure influence on the extraction yield under the following operating conditions: temperature (T) = 313.15 K, solvent flow rate (Q) = 5.88 kg/h,

cosolvent concentration (CS) = 7.8 wt. %, particle size (d_p) = 0.68 mm, and solid particle weight (w) =100 g (Zuo et al., 2008).

The higher fluid density enhances the solubility of isoflavones in modified $SCCO_2$ with increasing pressure (Figure. 4.29). This, in turn, favours the extraction process but is offset to some degree by a decrease in the diffusion coefficient, leading to reduction in the penetration capacity of the solvent and the extraction yield at higher pressures. As can be seen in Table 4.12 and Figure 4.30, effective diffusivity and mass transfer coefficient decreased but solubility of isoflavones and axial dispersion coefficient increased with pressure. In other words, the internal and external mass transfer resistances showed a negative effect on extraction yield. Extraction yield increased with increasing pressure. The result showed that at the increasing pressure, the positive effects on the isoflavone extraction overcame the negative effects.

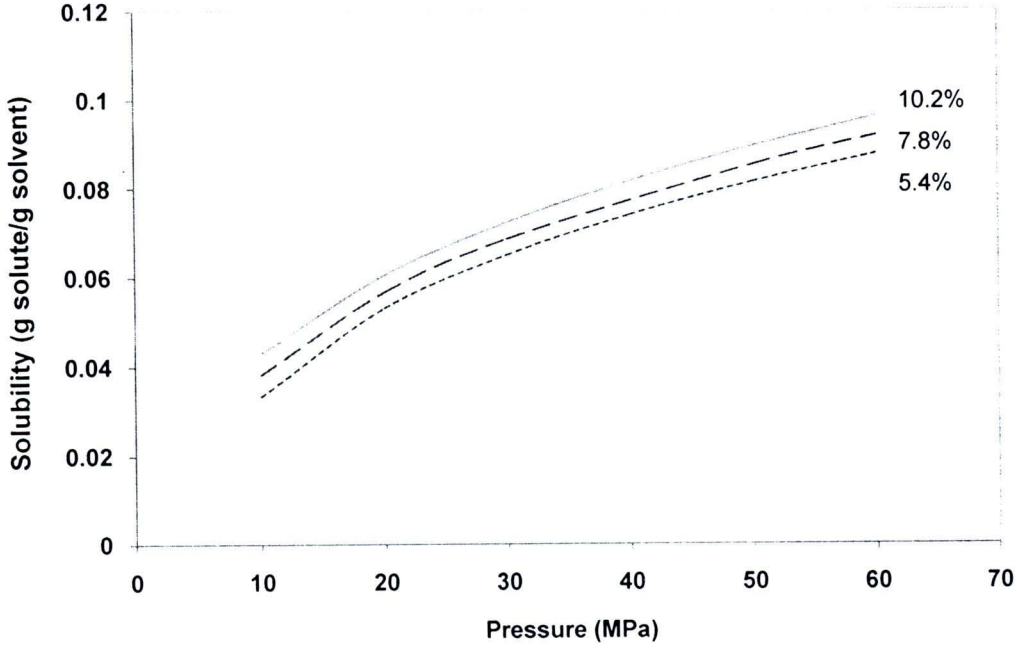

Figure 4.29 Solubility of isoflavones in supercritical CO_2 as a function of pressure and modifier (80% aqueous methanol) concentration at T = 313.15 K.

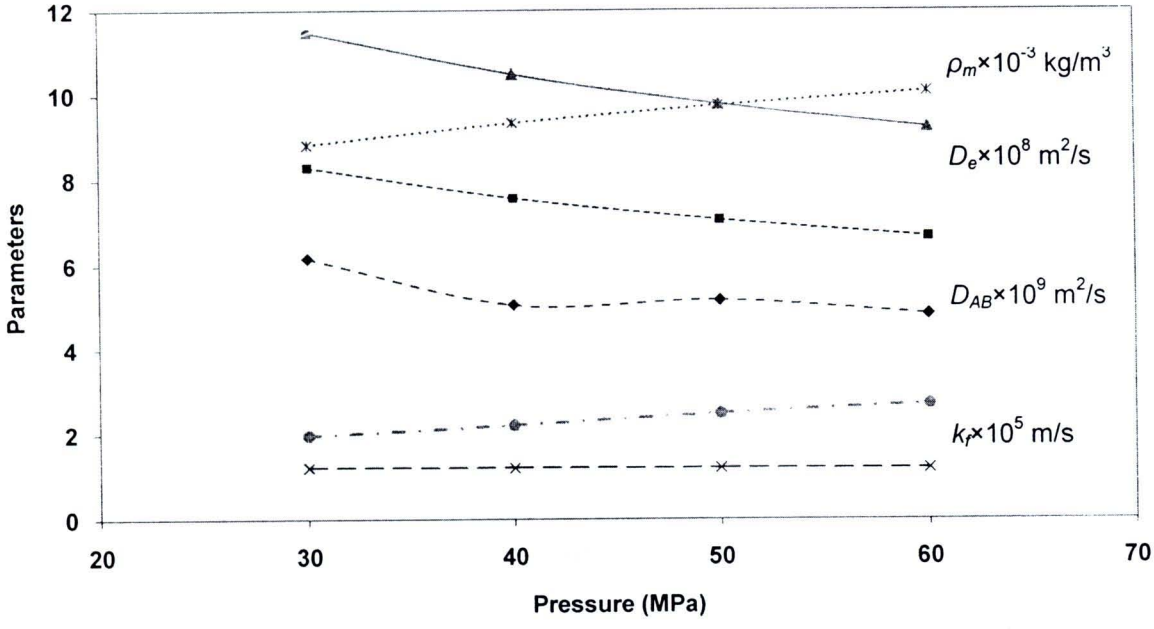

Figure 4.30 Effects of pressure on the transport properties of isoflavones in soybean at T = 313.15 K, Q = 5.88 kg/h, CS = 7.8 wt. %, d_p = 0.68 mm, and w =100 g (Zuo et al., 2008).

4.3.1.2 Effect of Temperature

Figure 4.31 illustrates that increasing temperature showed a negative effect on isoflavones extraction at 50 MPa. Higher temperature resulted in lower extraction yield. The effect of temperature on extraction rate was more difficult to assess than the effect of pressure, and represented a trade-off between increasing solute vapour pressure and decreasing mixture density as temperature increased. As temperature increases, mixture density deceases, leading to reduction in extraction yield. On the contrary, the increase in the vapour pressure enhances the solubility of the isoflavones more favourable as shown in Figure 4.32. Furthermore, the internal and external mass transfer resistances decrease by the increase of effective diffusivity and film mass transfer coefficient (Figure 4.33 and Table 4.11). At 50 MPa, the temperature showed an inverse effect on the yield (Figure 4.31) where the solubility was dominant effect. In this case the change of the solute vapour pressure was less effective than that of solvent density. This assumption might be possible due to the same trend of experimental results obtained by Bensebia et al. (Bensebia et al., 2009) who showed that the overall mass transfer coefficient in the solid phase increased with temperature at 10 MPa, but decreases at 18

MPa. From Figure 4.31, the model was able to predict the extraction yield which was good agreement with the experimental data.

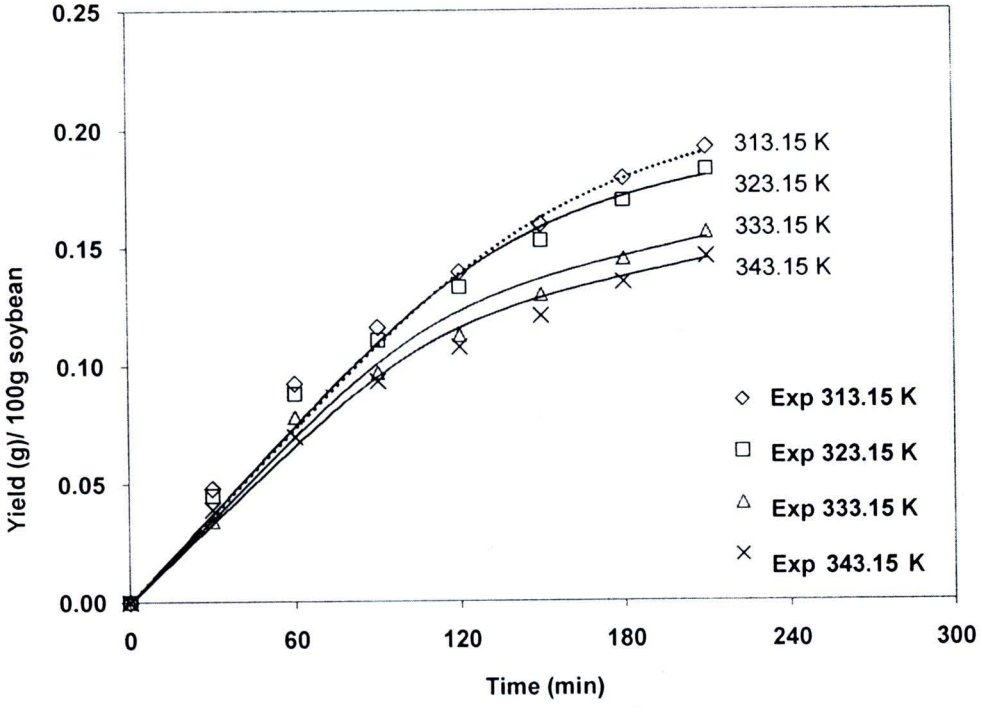

Figure 4.31 Temperature influence on the extraction yield under the following operating conditions: P = 50 MPa, Q = 5.88 kg/h, CS = 7.8 wt. %, d_p = 0.68 mm, and w =100 g (Zuo et al., 2008).

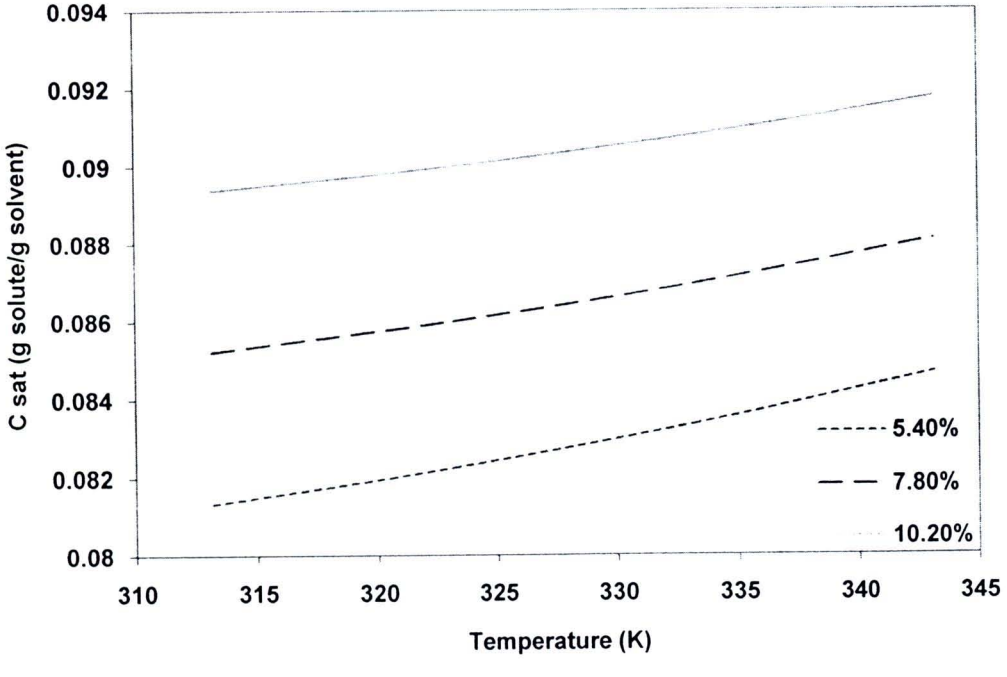

Figure 4.32 Solubility of isoflavones in supercritical CO_2 as a function of temperature and modifier (80% aqueous methanol) concentration at: P = 50 MPa.

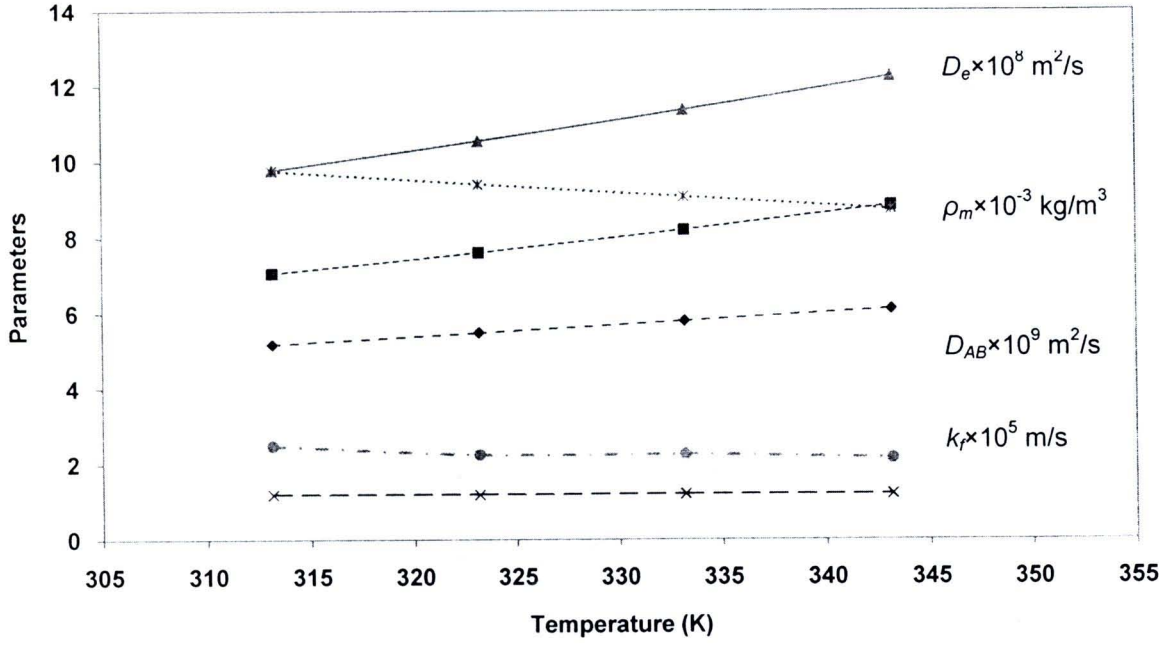

Figure 4.33 Effects of temperature on the transport properties of isoflavones in soybean at P = 50 MPa, Q = 5.88 kg/h, CS = 7.8 wt. %, d_p = 0.68 mm, and w =100 g.

4.3.1.3 Effect of CO_2 Flow Rate

Figure 4.34 shows that four CO_2 flow rates produced different isoflavone extraction rates. The extraction rate and yield increased with an increase in CO_2 flow rate. The axial dispersion and film mass transfer coefficient increased with CO_2 flow rate while other parameters remained constant, as reported in Table 4.9 and Figure 4.35. In addition, the mass transfer resistance surrounding the solid particle becomes smaller, due to the increasing of convection. A high rate of dispersion hinders the extraction rate and efficiency; therefore, a moderate flow rate would be optimal. The optimum flow rate, however, depends on the nature of solvent-solute systems, temperature, pressure, and extractor geometry (Elkanzi and Singh, 2001). Based on this effect, the mathematical model satisfactorily described the experimental data.

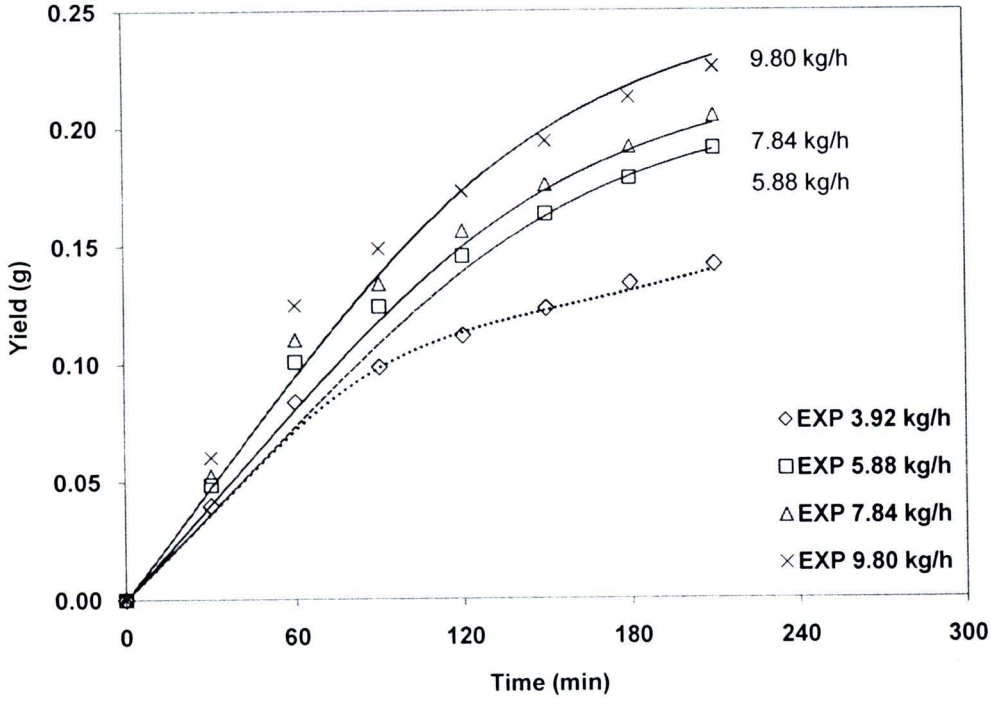

Figure 4.34 CO_2 flow rate influence on the extraction yield under the following operating conditions: P = 50 MPa, T = 313.15 K, CS = 7.8 wt. %, d_p = 0.68 mm, and w =100 g (Zuo et al., 2008).

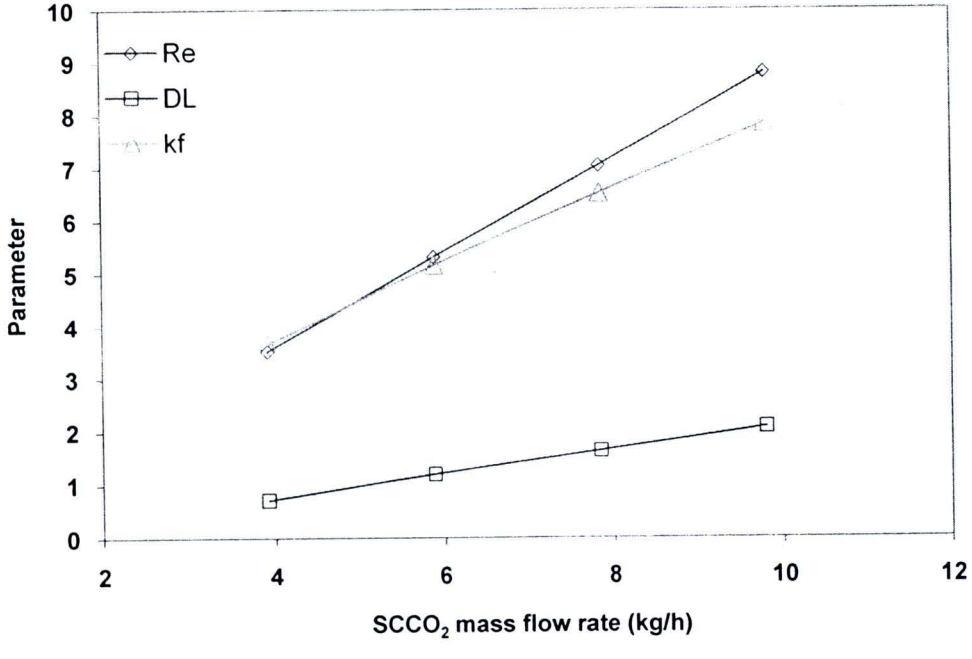

Figure 4.35 Effects of solvent mass flow rate on the transport properties of isoflavones in soybean at P = 50 MPa, T = 313.15 K, CS = 7.8 wt. %, d_p = 0.68 mm, and w =100 g.

4.3.1.4 Effect of Cosolvent Concentration

Figure 4.36 reveals the effect of the cosolvent concentration on the extraction efficiency of isoflavones. Extraction yield tended to increase as much as cosolvent concentration increased. As expected, addition of a polar cosolvent such as ethanol (Özkal, Yener and Bayındırlı, 2005) or methanol (Bensebia et al., 2009) caused a great influence on the better extraction behaviour and permitted to reach higher global yields. The cosolvent effect was dependent on the concentration of the cosolvent in the supercritical phase, which was determined by the phase behaviour of the mixture under operating conditions. Even though, all parameters except the solubility (Figure 4.37) tended to reduce the extraction yield as modifier concentration increased (Table 4.9). The mixture density also decreased with increasing cosolvent amount. The addition of cosolvents (e.g. methanol or water which has a higher molar volume than that of CO_2) to the SCF, diminishes the molar density of the solvent (Dobbs, Wong and Johnston, 1986). Intermolecular interactions are implied to be the major factors affecting isoflavones yield. Increasing amounts of cosolvent may fracture the cellular wall which, in turn, improves the mass transfer inside the cells (Sovová, Stateva and Galushko, 2001). As a result, a good agreement between the experimental yield and the predicted yield was observed (Figure 4.36).

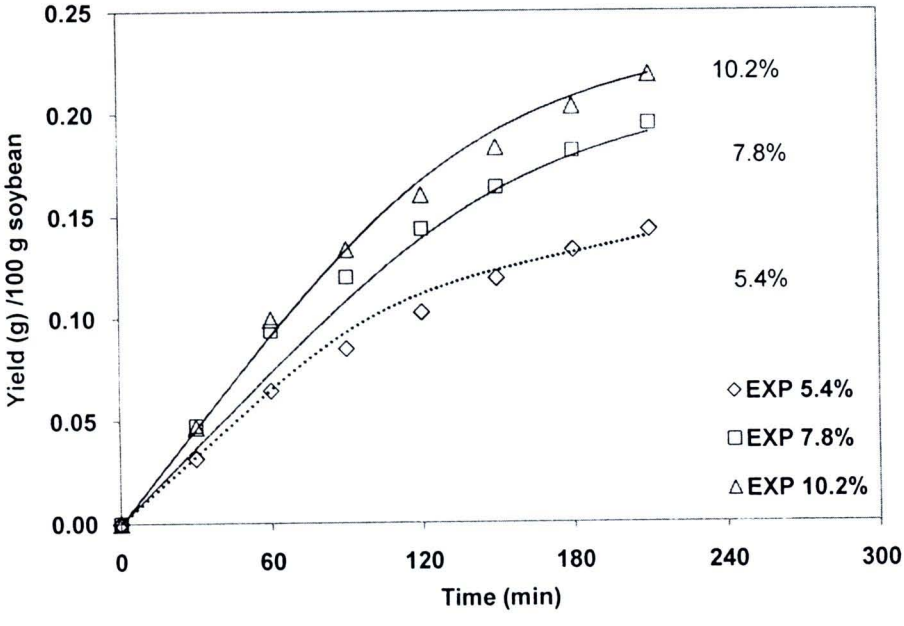

Figure 4.36 Effects of modifier (80% aqueous methanol) concentration on the extraction yield under the following operating conditions: P = 50 MPa, T = 313.15 K, Q = 5.88 kg/h, d_p = 0.68 mm, and w =100 g (Zuo et al., 2008).

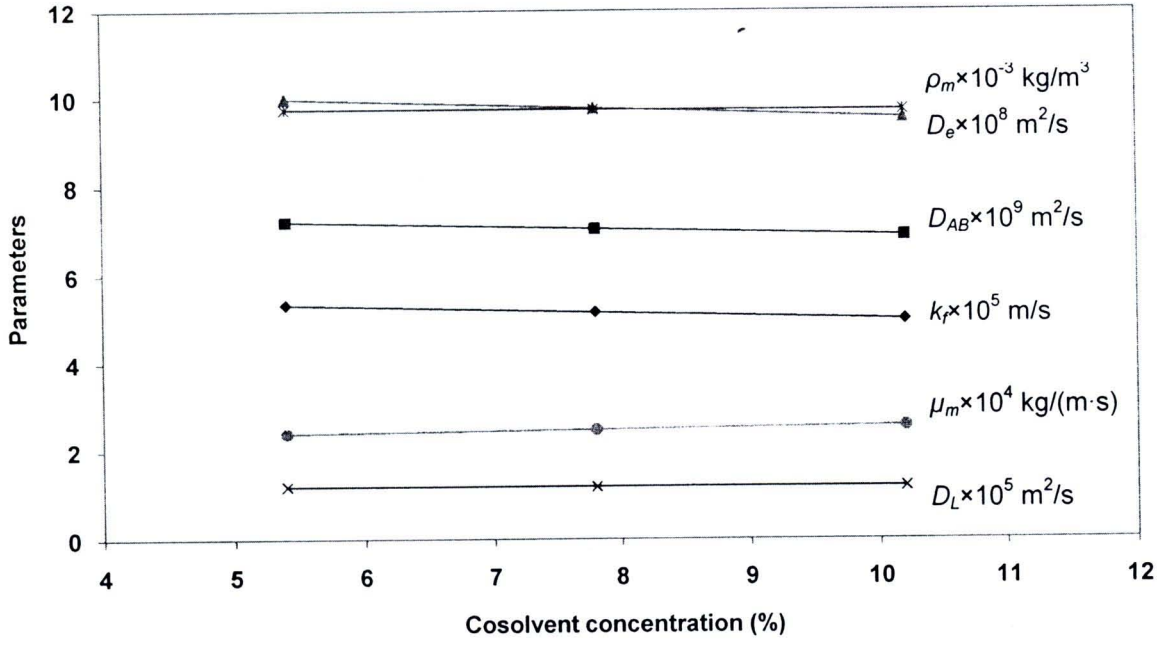

Figure 4.37 Effects of cosolvent concentration on the transport properties of isoflavones in soybean at P = 50 MPa, , T = 313.15 K, Q = 5.88 kg/h, d_p = 0.68 mm, and w =100 g (Zuo et al., 2008).

4.3.1.5 Effect of Particle Size

Figure 4.38 shows the variation of extraction yield with particle size (0.48-1.19 mm). Generally, the grinding process produces smaller particle sizes, which increase surface area. Not only the diffusion path is shorter but also intraparticle diffusion resistance is reduced. All of which result in extraction yield enhancement. This fact can be described well with the particle size ranging between 0.68-1.19 mm. However, very small particles (d_p < 0.68 mm) result to compact extraction beds, which cause solvent channelling in the extractor, thus reducing the extraction efficiency (Reverchon and Marrone, 2001). From this point of view, an optimal particle diameter is possible. The effective diffusivity coefficient plays an important role in the particle size effect. In this case, the optimal particle size should be around 0.68 mm because it provided higher yield than any other particle size. Even though the film mass transfer coefficient and axial dispersion coefficient were at the moderate values, the effective diffusivity coefficient was the higher than those of other particle sizes (Table 4.9).

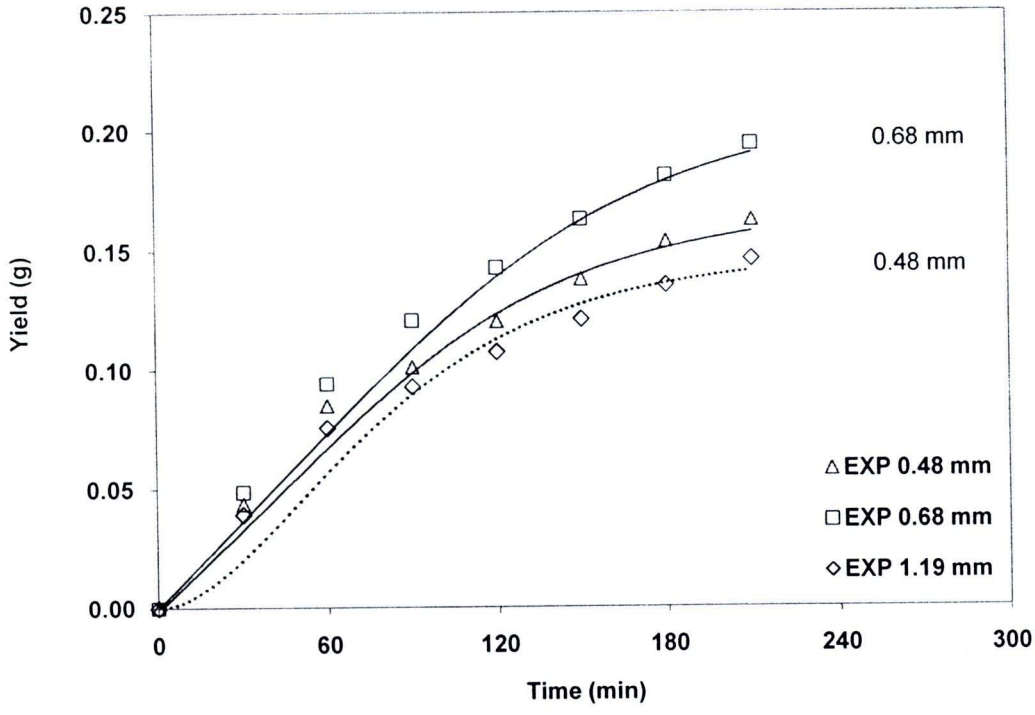

Figure 4.38 Effects of particle size on the extraction yield under the following operating conditions: P = 50 MPa, T = 313.15 K, Q = 5.88 kg/h, CS = 7.8 wt. %, and w =100 g (Zuo et al., 2008).

In conclusion, an increase in the pressure, the $SCCO_2$ flow rate, and the cosolvent concentration improved the extraction yield and also reduced the extraction time. The extraction yield increased as the particle size and the temperature decreased. The model can satisfactorily describe experimental observations, and the overall average absolute relative deviation (AARD) is about 6.54%.

In this work, there are other two operating parameters to be considered: bed height and extraction time. The effect of bed height cannot be investigated due to the limitation of the experimental information. Berna et al. (Berna et al., 2000) experimentally examined the influence of the bed height on the extraction rate with different amounts of a raw material and at various scales. All experiments resulted in similar extraction rates. Thus, this effect was assumed to be negligible. In the case of extraction time, all simulation results indicated that extraction yield increased with extraction time and asymptotically converged on an equilibrium yield. Therefore, to estimate an optimum extraction time, it is necessary to know the effect of extraction time on the operating cost of the process. Based on Run no. 3 condition, Figure 4.39 shows the predicted isoflavones content in

the $SCCO_2$ leaving a single extractor with the extraction time of more than 210 min. The outlet solute concentration remained constant after an initial period elapsed (the first 100 min), then, the concentration rapidly decayed and reduced to very low value after 400 min (internal mass transfer limiting step).

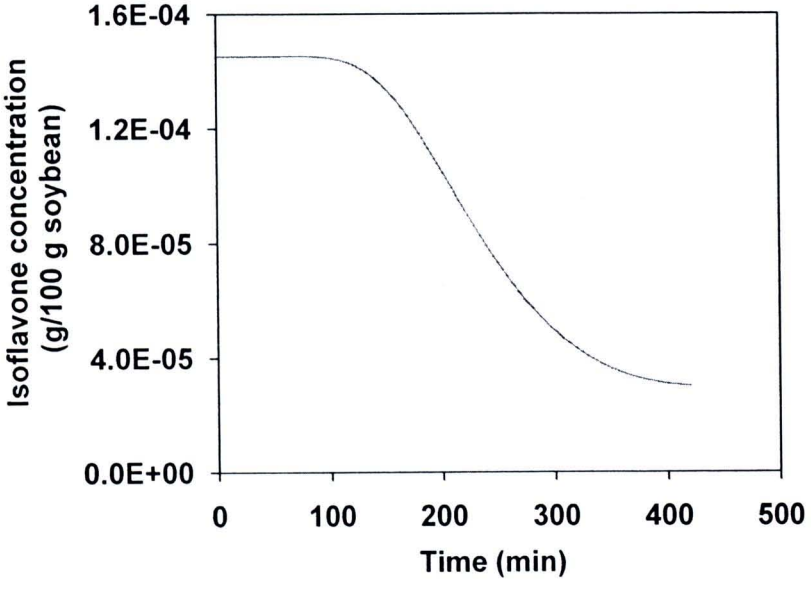

Figure 4.39 Predicted concentration of isoflavones at the outlet of an extractor during the extraction process (Run no. 3).

All extraction yield profiles of these relationships behave according to their physical meaning as evident in Table 4.14. This table summarises the effects of raw material features, the extractor geometry, and processing parameters on the extraction yield. Some input parameters have a direct and clear impact on the extraction yield such as $SCCO_2$ flow rate. For instance, increasing solvent flow rate results in increased Reynolds and Sherwood numbers and as a consequence, decreases the extraction time to reach a specific yield. However, for some other input parameters, their effects on the extraction yield cannot be predicted without additional analysis. Indeed, when the input parameter is involved in more than one dimensionless variable, a careful analysis is required. This is necessary when the input parameter has been opposing effects on the extraction yield, such as particle size.

Table 4.14 Prediction of extraction yield as a function of the input parameters.

Inputs			Direction variation	Intermediate inputs										Dimensionless inputs							Y
				ρ_m	μ_m	D_{AB}	v_f	ε_b	a_v	k_f	D_e	D_L	C_{sat}	a	b	Bi	Re	Sc	Sh	Pe	
Materials to be extracted	d_p		↑	–	–	–	↑	↑	↓	↓	↑↓	↑	–	↑	–	↑	↑	–	↑	↓	↓↑
			↓	–	–	–	↓	↓	↑	↑	↓↑	↓	–	↓	–	↓	↓	–	↓	↑	↑↓
Extractor vessel	D		↑	–	–	–	↓	↑	–	↓	–	↓	–	↓	–	–	–	–	↓	↓	↓
			↓	–	–	–	↑	↓	–	↑	–	↑	–	↑	–	–	–	–	↑	↑	↑
	L		↑	–	–	–	–	↑	–	–	–	↑	–	↓	–	–	–	–	↑	↑	↑
			↓	–	–	–	–	↓	–	–	–	↓	–	↑	–	–	–	–	↓	↓	↓
Operating conditions	T	low P	↑	↓	↑	↑	↑	–	–	↑	↑	↑	↑	–	↑	↓	↑	↓	↑	↓	↑
			↓	↑	↓	↓	↓	–	–	↓	↓	↓	↓	–	↓	↑	↓	↑	↓	↑	↓
		high P	↑	↑	↓	↑	↑	–	–	↑	↓	↓	↑	–	↑	↓	↑	↓	↓	↓	↓
			↓	↓	↑	↓	↓	–	–	↓	↑	↑	↓	–	↓	↑	↓	↑	↑	↑	↑
	P	low T	↑	↑	↑	↓	↓	–	–	↓	↓	↓	↑	–	↑	↓	↓	↑	↓	↑	↑
			↓	↓	↓	↑	↑	–	–	↑	↑	↑	↓	–	↓	↑	↑	↓	↑	↓	↓
Solvent flow rate	Q		↑	–	–	–	↑	–	–	↑	–	↑	–	↑	–	↑	↑	–	↑	↓	↑
			↓	–	–	–	↓	–	–	↓	–	↓	–	↓	–	↓	↓	–	↓	↑	↓
Cosolvent concentration	CS		↑	↓	↑	↓	–	–	–	↓	↓	↓	↑	–	↑	↓	↓	↑	↓	↑	↑
			↓	↑	↓	↑	–	–	–	↑	↑	↑	↓	–	↓	↑	↑	↓	↑	↓	↓

4.3.2 Sensitivity Analysis

Sensitivity analysis is important to determine the influence of changes in inputs on changes in outputs. Parameters that the model is highly sensitive to may require more research to determine accurate parameter estimations. Simulations were carried out by varying one parameter at a time while keeping all other parameters constant at their base case values (Run no. 3 as shown in Table 4.12). A reference parameter value (p_r) was assigned to each model parameter. Simulations were performed over the range $0.2p_r \leq p_r \leq 2p_r$. Then, the sensitivity analysis results were plotted in Figure 4.40-4.41.

4.3.2.1 Effect of Solvent Flow Rate

The solvent flow rate effect was investigated; as can be seen in Figure 4.40, the extracted yield was not always proportional to the increase in the quantity of CO_2, particularly in the solubility controlled region. The curves moved to the left along with a solvent flow rate, which means that the overall extraction is faster and approach to the same maximum yield (≈ 90% of total isoflavones extracted). This result indicated that the model depends strongly on the solvent flow rate.

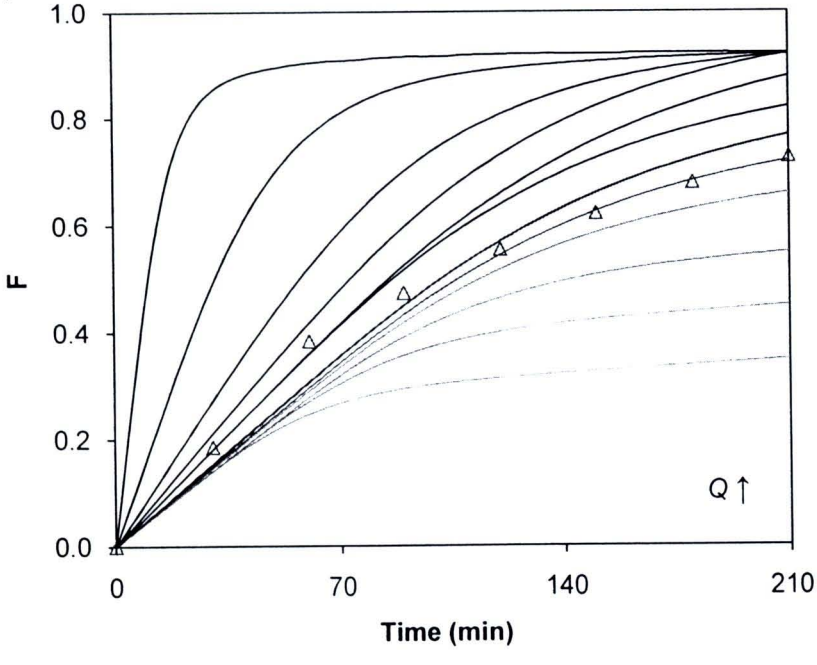

Figure 4.40 Effect of solvent flow rate on extraction plots (△: EXP).

4.3.2.2 Effect of Mixture Density

The density and viscosity were assumed to be constant (over time) and only to be functions of temperature and pressure. However, the density will likely change due to the concentration gradient that exists as the solute from solid seed diffuses to the bulk phase (fluid). Figure 4.41(a) reveals the effects of mixture density on the yield, indicating that the sensitivities are relatively larger at low rather than high values of the mixture density. However, the predicted yields were found to be insensitive to mixture density.

4.3.2.3 Effect of Mixture Viscosity

The relatively high and reversibly adjustable density makes SCFs ideally suitable for simultaneous extraction and fractionation of various solutes and their relatively low viscosity provides appreciable penetrating power into the solute matrix. Normally, the mixture viscosity increases with increasing pressure and decreasing in temperature. Figure 4.41(b) shows that, although, the yield deviation was larger at a low mixture viscosity than at high mixture viscosity, the viscosity had a relatively low sensitivity on the overall extraction yield.

4.3.2.4 Effect of Film Mass Transfer Coefficient

The film mass transfer coefficient in the fluid phase increases with decreasing pressure and increasing solvent velocity. In the model, this parameter is represented in terms of the Biot number in Equation 3.66. Figure 4.41(c) shows that extraction curves are highly sensitive to this parameter, derived from Tan et al. correlation. A good estimate of the film mass transfer coefficient is vital for the design or sizing of an extractor since its value regulates the rate of mass transfer during the extraction process.

4.3.2.5 Effect of Effective Diffusivity

The most important parameter that controls the diffusion of solute in the particle pores is the effective diffusion coefficient. This parameter is used to describe the mass transfer within the extracted solid and usually selected to be a fitted parameter in many proposed models. It increases with decreasing particle size. Figure 4.41(d) shows that the model is quite sensitive to the effective diffusion coefficient. A small discrepancy in of this parameter results in a significant change in the yield.

4.3.2.6 Effect of Axial Dispersion Coefficient

With regards to our assumption, dissolved solute in the SCF diffuses along the bed (dispersion coefficient) as a result of axial concentration gradients. If relatively large particles are used, mass transfer due to axial dispersion might be taken into account (Abaroudi et al., 1999). The experimental data indicated that the axial dispersion coefficient is a function of temperature, pressure, and flow rate. This parameter decreases with increased temperature and pressure due to the increase of density and viscosity of the $SCCO_2$. Furthermore, the axial dispersion coefficient increased with increasing interstitial velocity as depicted in Table 4.12. Simulation results (Figure 4.41(e)) showed that this effect is very small. These results implied that the SFE process does not rely on axial dispersion to obtain high performance.

4.3.2.7 Effect of Solubility

The solubility of solute in the supercritical fluid not only depends on pressure and temperature but also on the modifier concentration (Figure 4.29 and 4.32). The solubility depends on a complex balance between SCF density and solute vapour pressure, which are both controlled by the fluid pressure and temperature. In addition, the cosolvent concentration also tends to increase solubility (Table 4.12). To calculate the solute concentration and core radius with time, the solubility must be known. It was expressed in terms of a parameter b, included in Equation (3.66) - (3.67). The integral extraction plot in Figure 4.41(f) clearly showed that changes in the solubility had a significant effect on the extraction yield.

All parameters had a positive effect on the predicted yield except the mixture viscosity and the axial dispersion coefficient as shown in Figure 4.41. For these two parameters, this happens in a real situation because the increase of the mixture viscosity and the axial dispersion coefficient result in higher mass transfer resistance. Among all parameters evaluated, it is noticeable that the model predicted F exceed its maximum value ($F = 1$) when the film mass transfer coefficient and the solubility were tended to increase as shown in Figure 4.41(c) and 4.41(f). In case of the solubility, this was obviously explained by the parameter b multiplied with the integral term of Equation 4.68. If the solubility was increased as a consequence b was also increased. Then, the model produced higher extraction yield, which might be overestimated. In case of the film mass transfer coefficient, it was represented in terms of the Biot number appeared

in the last term on the right hand side of Equation 3.66. Similarly, the Biot number was increased with the film mass transfer coefficient then the value of this last term also became larger. This tended to get higher predicted yield. The film mass transfer coefficient and the solubility are the most sensitive parameter. Therefore, the risk of error in these parameters will dominate the error in the result. To minimise the error between predicted and measured yield over time, the most sensitive parameters are always required to be more accurate.

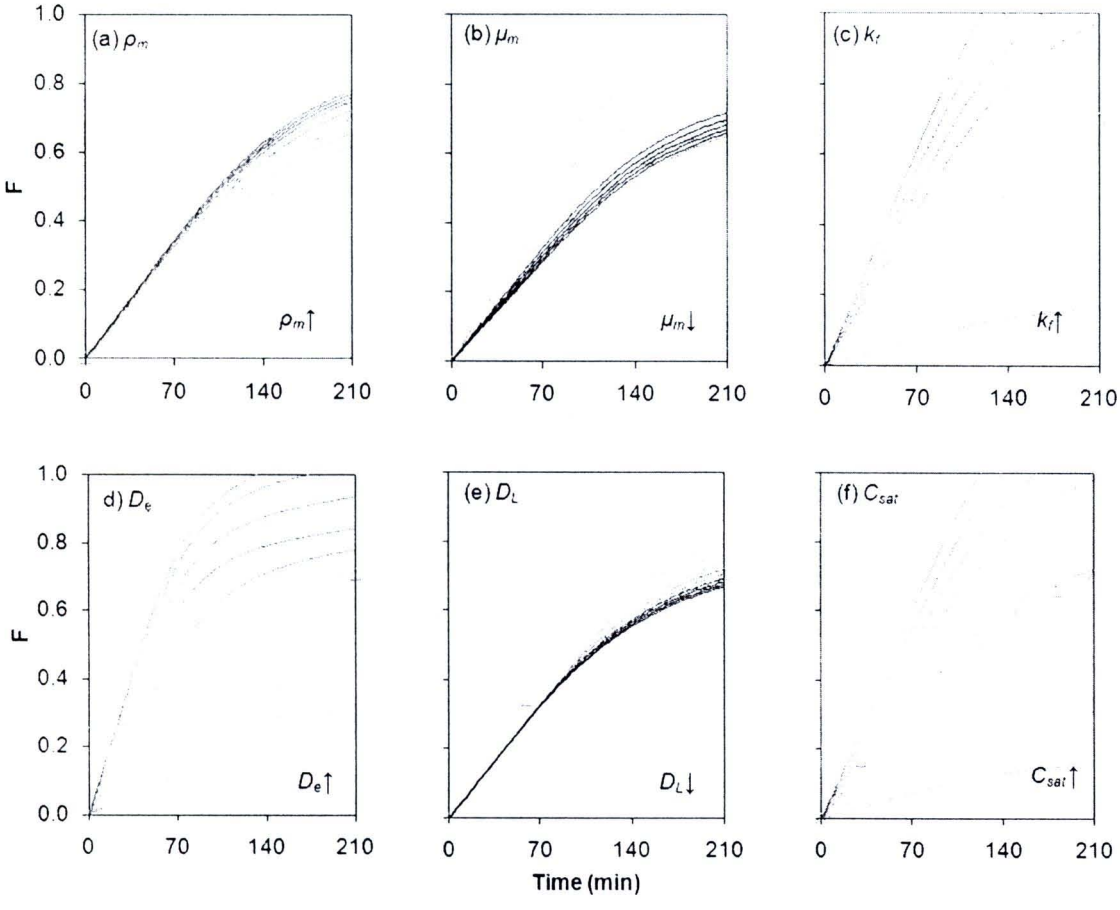

Figure 4.41 Effects of parameters on extraction plots: (a) ρ_m, (b) μ_m, (c) k_f, (d) D_e, (e) D_L, and (f) C_{sat} (Δ: EXP).

To rank the effect of uncertain model parameters on predictions, the model sensitivity, $s(p)$ to the parameter (p) variations was also analysed using the Ratto et al. correlation (Ratto, Lodi and Costa, 1996), Equation 4.1. This led to the evaluation of the uncertainty of the model output, $e(p)$ resulting from the uncertainty of input parameters, $i(p)$ in Equation 4.2 - 4.3.

$$s(p) = \frac{d[\tau(p)]}{dp} \cdot \frac{p}{\tau(p)} \quad (4.1)$$

$$i(p) = \frac{\Delta p}{p_r} \quad (4.2)$$

$$e(p_r) = i(p_r) \cdot s(p_r) \quad (4.3)$$

where $i(p)$ and $e(p)$ are the uncertainty function of the input and output parameters, respectively.

To perform this analysis, the target function was an extracted isoflavones yield equal to 0.1857 g/g. The analysis gave a reference to the process time (τ_r) corresponding to the achievement of this target. After that, the uncertainty of input parameters was estimated from the error of measurement (Fiori, Calcagno and Costa, 2007). Table 4.10 summarises the sensitivity result referred to τ_r = 210 min. The model prediction was found to be sensitive to the model parameters, ranked in descending order: the film mass transfer coefficient, the solubility, the effective diffusivity, the solvent flow rate, the axial dispersion coefficient, the mixture viscosity, and the mixture density, respectively.

Table 4.15 Sensitivity and effects of parameter uncertainty.

Parameter	$s(p_r)$	$i(p_r)$, %	$e(p_r)$, %
Q	0.954	±20	19.08
ρ_m	0.314	±3	0.94
μ_m	0.437	±3	1.31
k_f	4.019	±10	40.19
D_e	1.329	±20	26.58
D_L	0.388	±40	15.52
C_{sat}	3.702	±10	37.02

From a practical point of view, the mixture density, mixture viscosity, and axial dispersion coefficient can be neglected from further investigation since their values have little effect of the extraction yield. As well the solvent flow rate is specified by the

user and therefore, well known. However, the film mass transfer coefficient and solubility were found to be particularly important.

4.4.3 Extractor Configuration

The cyclic-batch operating mode using fixed bed, as shown in the Figure below, is widely used with both gas and liquid feeds. Separation in a fixed bed is, in virtually all practical cases, an unsteady state rate-controlled process. This means that conditions at any particular point within the fixed bed vary with time. Extraction only occurs in a particular region of the bed, known as the mass transfer zone (MTZ), which moves through the bed. As fluid is passed through the fixed bed of solid, the transfer of molecules from the solid to the feed fluid initially occurs at the bed entrance. The MTZ then progressively move through the bed once the supercritical fluid in a region becomes saturated with the solute molecules. Thus at any instant in time, the fluid upstream or downstream of the MTZ do not participate in the mass transfer processes. Upstream of MTZ, the fluid is already saturated and in equilibrium with the feed, and unable to extract further solutes. Downstream of MTZ, the fluid is not yet in contact with any solutes. Thus, despite having the capacity of extraction will be unable to do so. Thus, if the time required for the progress of MTZ through the bed is long, the bed will be large. The pressure drop across the bed will also be proportionately large.

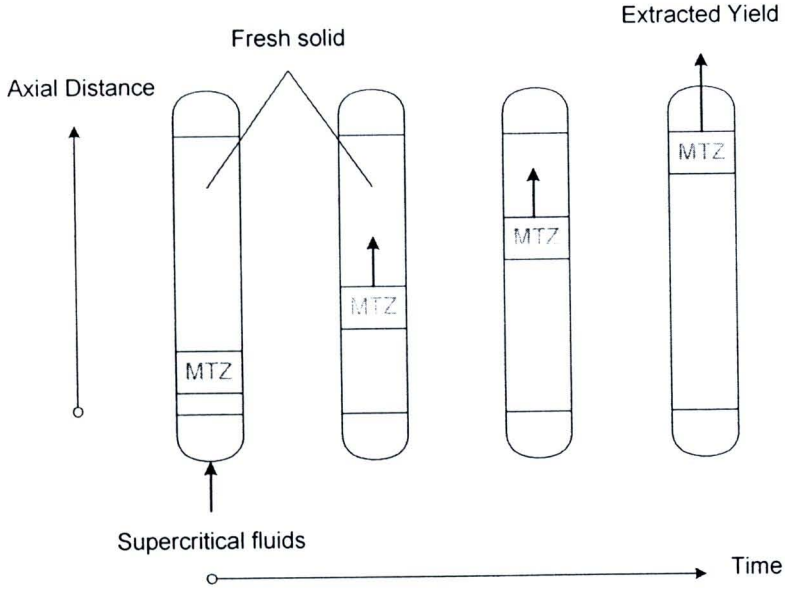

Figure 4.42 Mass transfer zone in the fixed bed (Brunner and Johannsen, 2006).

The factor which determine the number and arrangement of fixed bed include total feed flow rate, allowable pressure drop, energy demands, length of MTZ, method of recovery, and the capital investment. In the initial part of the extraction, for example, when the yield curve is a straight line, the concentration at the extractor outlet remains constant and equal to the solubility value. In this case to save time, a large solvent flow rate is preferable. On the contrary, after this phase, the mass transfer kinetic of the solute inside the seed particle becomes the controlling step of the extraction process. In this case the solvent flow rate could be lowered, with only a slight increase in the process time but with a major reduction in solvent consumption (and energy cost saving). A control loop can be utilized for this purpose: a solute concentration sensor placed at the extractor outlet.

A single-extractor plant cannot produce isoflavones continuously. In order to achieve a steady state flow of product, most applications include at least 2 beds due to the fixed time which must be devoted to the loading and unloading of solids, and the decompression and recompression of an extraction unit altogether require 10 min, as estimated by Caputo (1997). The packed beds can be connected in series, parallel, and series of parallel. Multiple beds in parallel would be used with a relatively high flow rate and a short MTZ length while multiple beds in series would be used if the MTZ were long. For high flow rates and large MTZ lengths the choice is likely to be multiple beds in series and parallel. In practice, more than 2 beds are often used which introduces the need for complex piping and valve arrangements together with a control system. In unique process application, where the contact time is several hours, three beds in series may be necessary. There are very few systems with four vessels in series. In a plant configuration with multiple extractors in parallel, it should be possible to work with the same total flow rate but varying the flow rate to the individual extractors, with a slightly more complicated system. A solute concentration set point has to be specified, then, when the measured solute concentration differs from its set point value, the controller opportunely modifies the solvent flow rate.

The following quantities were kept constant during comparing: the size of each extraction vessel, packed solid amount, temperature, pressure, cosolvent amount, cosolvent type, and the circulating solvent flow rate (and it residence time inside the

extraction vessels) as shown in Table 4.16. There are three cases which are studied as following.

Table 4.16 Main characteristics and operating conditions.

Operating Conditions	Value	Unit
Raw material (soybean meal) weight	100	g
Supercritical CO_2 flow rate	5.88	kg/h
Modifier flow rate	0.6	L/h
Total flow rate	1.83E-06	m^3/sec
Temperature	40	°C
Pressure	50	MPa
Extraction time	210	min

4.4.3.1 Single extractor

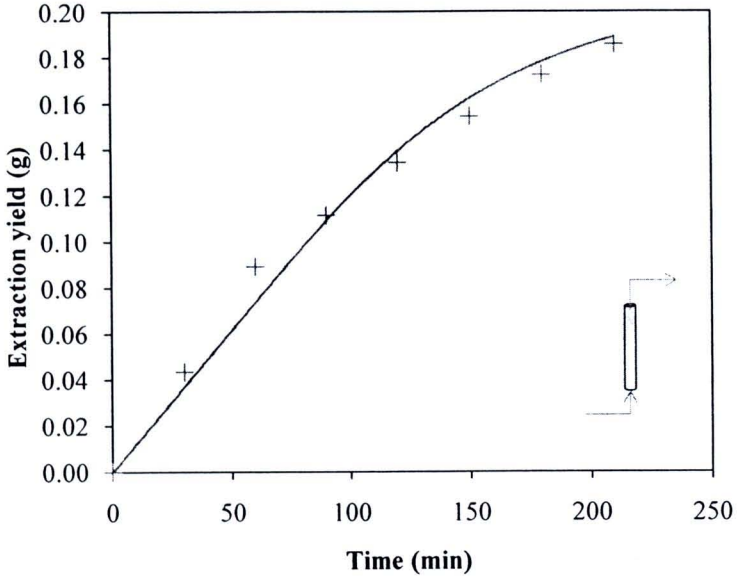

Figure 4.43 The extraction yield profile in an extractor with time.

The first 400 min of the time profile of the yield of a single extraction unit, considered independently of any other piece of equipment, were simulated to calculate the expected instantaneous isoflavones yield of an operating extractor as a function of the time past

since the beginning of the $SCCO_2$ flow. The time profile of the isoflavones content in the $SCCO_2$ stream leaving a single extractor during each extraction phase is shown in Figure 4.43 in previous section which is clearly shows that, after an initial period (the first 100 min of the extraction) where the outlet solute concentration remains constant (first part of the extraction curve). This quantity rapidly decays and reduces to very low values after 400 min (internal mass transfer limiting step).

4.4.3.2 Two extractors in series

Two stage series operation to provide longer contact and more complete extraction of solute is preferred. In series operation, the unit with freshest supercritical fluid at any given time should be in the lag and standby units should be provided. In another word, passing all of the flow through one column bed, a lead column, and then passing flow through another similar sized column bed, the lag vessel. This method offers several advantages over a single column. The series configuration allows the maximum use of the solid throughout the entire solid vessel. This assumes, of course, that the MTZ is contained within a single properly sized solid unit. By placing two or more columns in series, The MTZ is allowed to pass completely through the first (lead) bed as the leading edge of the MTZ migrates into the second (lag) bed. However, it is possible that the mass transfer zone may be contained in the first extractor in system having two extractors in series. As the process behaviour is influenced by the design flow rate is shown in Figure 4.44. All the profiles of these relationships behave according to their physical meaning. All the conditions are those of the reference case except the solvent flow rate, which is varied in the different simulation. Obviously, the greater the flow rate, the lower the process time and the greater the solvent consumption. In this analysis, we do not consider the pressure drops, which become important at relatively high flow rates. In our case study, the flow rate kept constant during the whole extraction will exist in the range of investigated. As depicted in Figure 4.45, two extractors in series with different flow rate (supercritical fluid) are compared such as 0.5 (case 3), 1 (case 4) and 2 (case 5) times of flow rates (5.88 kg/hr). As expected, the highest flow rate can obtain the extraction yield more than any other flow rate and gives the least residence time. This result is also obtained by comparing case 1 and 3.

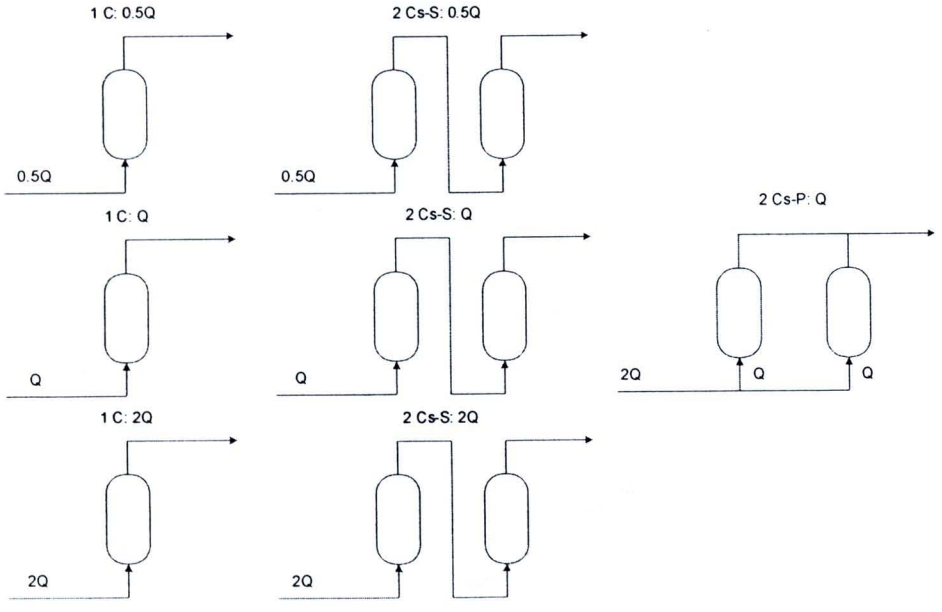

(a) Single column (b) Two columns in series (c) Two columns in parallel

No. of column	Arrangement type
1C =a column	S = series
2 Cs= two columns	P = parallel

Figure 4.44 Single, series and parallel extractor arrangements

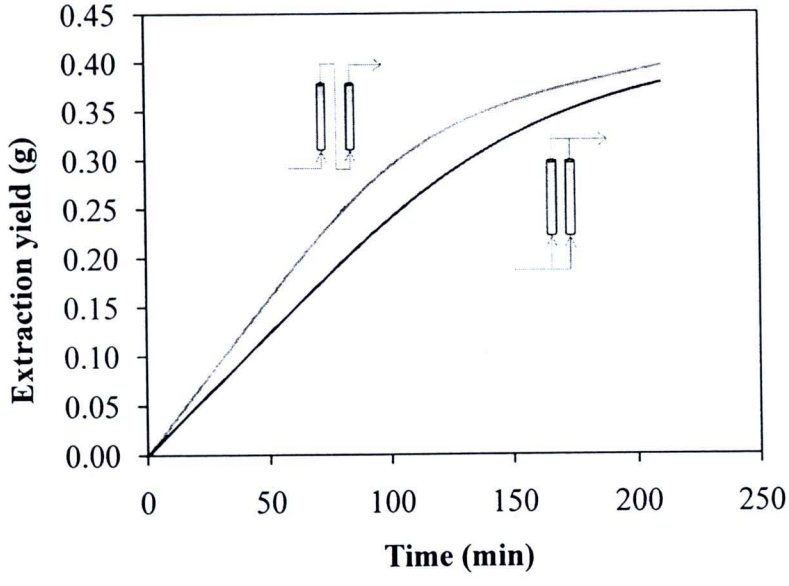

Figure 4.45 The extraction yield profile in two-extractors with time.

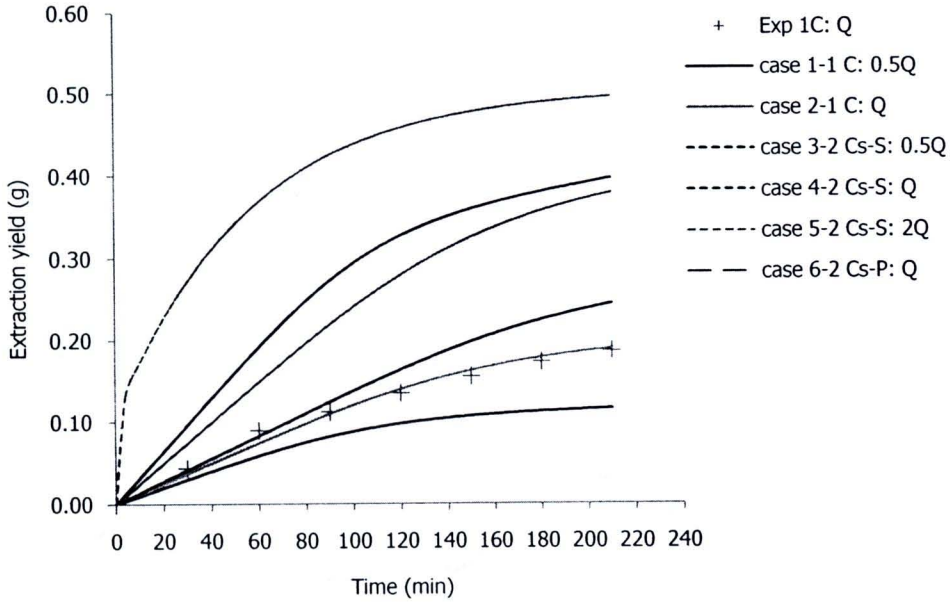

Figure 4.46 Comparison the predicted extraction yield profiles with time between three configurations and the experimental data (Zuo, 2008).

4.4.3.3 Two extractors in parallel

Multiple units in parallel arrangements are frequently used for high flow rates and increase the overall extraction capacity of the system when short contact times are adequate. Single units should be used only in installations in which the system can be shut down for change out of the solid. Multiple smaller units containing the same amount of solid and providing equal contact time are usually preferable to single large unit. For multi-vessel systems, flexible piping is generally used to allow easy interchange between parallel or series configurations. As can be seen in Figure 4.44, the predicted result of both case (series and parallel) are almost the same and can reach the maximum solute within the solid. In case of the same velocity (case 2, 4 and 6), two extractors in series (case 4) can access the highest yield but the two extractors in parallel (case 6) can give the extracted yield more than the single extractor (case 2). This is due to the amount of packed solid in two extractors is double when comparing with a single vessel.

Table 4.17 Isoflavones yield for different extractor configurations.

Configuration	No. of column	Solid wieght (g)	Total flow rate (Q)	Residence time (Q/V)	Extraction yield (%)
Single 	1	100	0.5Q	0.5Q/V	42.83
		100	Q	Q/V	70.31
		100	2Q	2Q/V	93.92
Series 	2	200	0.5Q	0.25Q/V	25.92
		200	Q	0.5Q/V	40.71
		200	2Q	Q/V	71.23
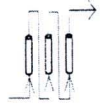	3	300	0.5Q	0.167Q/V	18.44
			1.5Q	0.5Q/V	41.86
			3Q	Q/V	70.55
Parallel 	2	200	Q	0.5Q/V	41.63
			2Q	Q/V	72.54
			4Q	2Q/V	90.91
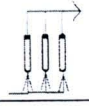	3	300	Q	0.33 Q/V	22.64
			3Q	Q/V	70.12